Enhancing climate resilience of vertical seawall with retrofitting - a physical modelling study

S. Dong[1], S. Abolfathi[1], M. Salauddin[1,2], Z. H. Tan[3], J. M. Pearson[1]

[1]Warwick Water Group, School of Engineering, University of Warwick, UK
[2]UCD School of Civil Engineering, UCD Dooge Centre for Water Resources Research, University College Dublin, Dublin 4, Ireland
[3]Environmental Change Institute, University of Oxford, UK

Abstract

Coastal defence structures are playing a vital role in protecting coastal communities from extreme climatic conditions and flooding. With climate change and sea-level rise in the next decades, the freeboard of existing coastal defences is likely to be reduced and the probability of wave overtopping for these coastal defences will increase. The wave overtopping from coastal defences increases the probability of coastal inundation and flooding, imposing threat to the communities which are living in low-lying coastal areas. Retrofitting of existing seawalls offers the potential to enhance coastal resilience by allowing them to adapt and respond to changing climatic conditions. This study investigates a range of possible physical configurations and optimum retrofit geometry to maximize the protection of existing seawalls from wave overtopping. A comprehensive physical modelling study of four retrofit prototypes, including recurve wall, model vegetation, reef breakwater and diffraction pillars, was conducted to examine their performance in mitigating wave overtopping, when placed in front of a vertical seawall. All the tests were conducted on 1:20 smooth beach slope. Each test case consisted of approximately 1000 pseudo-random waves based on the JONSWAP spectrum. The physical modelling experiments were designed to include both impulsive and non-impulsive wave conditions. This study provides new predictive relations and decision support tool needed to evaluate overtopping risks from existing seawalls with retrofits under various hydrodynamic conditions. The analysis of experimental measurements demonstrates that wave overtopping from retrofitting structures can be predicted with similar relations for vertical seawalls, and by using a reduction factor which varies with geometric shapes. Statistical measures and sensitivity analysis show that recurve walls have the best performance in reduction of wave overtopping volume followed by model vegetation and reef breakwater. The measurements show the insignificance of diffraction pillars, at least for the selected configurations investigated, in mitigating wave overtopping.

Keywords: overtopping discharge, wave-by-wave overtopping volume, coastal resilience, retrofitting seawalls, recurve wall, climate change adaptation, coastal flooding

1. Introduction

Coastal zones have been progressively developed in recent decades and have very significant socio-economic value to nations around the world. Protecting the coasts from natural hazards and in specific coastal flooding has been always a key area of research. Recent climate change studies (IPCC, 2014, 2018) show that not only the sea-level will continue to rise in the future, but more frequent extreme climatic events and coastal storm surges will occur in the near future, which could lead into catastrophic coastal flooding and inundation. Hence, challenges associated with protecting critical assets in the coastal region is exacerbated by the long-term effects of changing climate. Use of 'green infrastructure' in combination with traditional hard defences is an adaptable solution for enhancing the resilience of coastal area to extreme climatic conditions. Previous studies show that soft defences (e.g., re-creation of foreshores and beaches) can harmonize with the natural ecosystem, creating a self-healing system, and therefore have been rapidly finding favor over hard defences (Tusinski et al., 2014; Vuik et al., 2016). On the other hand, the existing hard defences are aging (Hall et al., 2017) and in the next decades with the sea-level-rise and increased frequency of extreme events, these defences will not be capable of providing sufficient level of protection. Therefore, it is vital to adopt engineering approaches such as 'retrofitting' of existing coastal defences, to enhance resilience of coastal defences.

Mean overtopping discharge is one of the key design parameters for coastal structures which is typically defined as the mean discharge per unit width of the structure (q). In recent decades, considerable efforts have been made for the development of robust predictive and decision support tools for evaluating mean overtopping discharge from coastal protection structures, in order to specify acceptable levels of overtopping. The existing predictive tools for overtopping are primarily based on the derivation of empirical equations from measured data (Allsop et al., 2005; Besley et al., 1998; Franco et al., 1995). However, the reliability of analytical approaches is often questionable as the dynamics in overtopping rarely resemble the well-controlled conditions presented in analytical studies. In recent years, advanced numerical techniques have also been adopted to quantify and predict performance of coastal infrastructures under various hydrodynamic and geometrical setups, as well as understanding complex flow-structure interactions influence on wave overtopping (Abolfathi et al., 2018; Abolfathi and Pearson, 2017; Yeganeh-Bakhtiary et al., 2017 & 2020).

Wave-structure interaction regimes tend to produce distinct structural responses to wave overtopping, and influence the overtopping discharge values. For incident waves approaching a steep wall, three distinct conditions including 'impulsive', 'non-impulsive' (or pulsating) and 'near breaking' conditions are possible. Under impulsive wave condition, the overtopping discharge could be characterized by a rapid jet of water at the toe of the structure. Under near-breaking conditions, overtopping is characterized by high-speed jet of water, but the wave breaking phenomena does not occur at the wall. The

resemblance between near-breaking and impulsive wave conditions allows the near-breaking conditions to be treated similarly to fully-impulsive conditions.

An early formulation for non-impulsive mean overtopping discharge was established by Franco et al. (1995), based on analysis of a series of two-dimensional physical model tests on caisson breakwater. Franco et al. (1995) empirical relation predict the non-impulsive mean overtopping discharge as an exponential function of relative freeboard. Besley et al. (1998) and Allsop et al. (2005) studied impulsive wave conditions and proposed empirical predictive formulae which estimate mean overtopping discharge as a power law function of relative freeboard.

Many studies have subsequently been performed to refine the predictions of mean overtopping discharge for both impulsive and non-impulsive wave conditions. The EurOtop (2018) manual for overtopping design, has provided a comprehensive review of wave overtopping studies, and by re-analysing previously measured data, the manual also explored the interplay between crest freeboard and mean overtopping discharge. EurOtop (2018) report that mean overtopping discharge measurements for structures with small to zero freeboard have well agreement with the prediction formulae using exponential function, whilst for large freeboards, overtopping is best described by equations using power law function. van der Meer and Bruce (2013) suggested a unified scheme to compare the mean overtopping discharge for both impulsive and non-impulsive regimes.

Recent improvements in predictive tools for evaluating mean overtopping discharge from coastal defences have motivated number of studies to examine the effectiveness of retrofitting structures, such as recurve walls and reef breakwaters, in reducing wave overtopping from coastal structures (Dong et al., 2018; Kortenhaus et al., 2003; Van Doorslaer et al., 2016). A number of studies investigated the effects of recurve retrofitting structures on the mean overtopping discharges from various types of coastal defenses (Molines et al., 2019a; Pearson et al., 2004; Van Doorslaer and De Rouck, 2011). The performance of recurves, described by the mean overtopping discharge, is found to be sensitive to recurve structural dimensions, including overhang length and height (Formentin and Zanuttigh, 2019a; Kortenhaus et al., 2002) and the recurve angle (Martinelli et al., 2018; Van Doorslaer et al., 2015). The literatures suggest long overhang length and recurve angle of ~45 degree have the most promising mitigating performance and structural stability.

Vuik et al. (2016) studied the performance of vegetated foreshores on coastal dikes and suggested that presence of vegetation in the foreshore region lead into an additional 25 to 50 percent reduction in significant wave height for breaking wave conditions. The recent laboratory work by Salauddin and Pearson (2019) and (2020) on permeable foreshore slopes in front of vertical seawalls and sloping dikes showed that mean overtopping characteristics are reduced significantly, when compared to the impermeable foreshore in front of the sea defences. Furthermore, laboratory investigations on the wave overtopping characteristics at ecologically enhanced sea defences showed that eco-retrofitting can enhance the climate resilience of critical coastal infrastructures by mitigating extreme wave overtopping, particularly for impulsive wave attack (Salauddin et al., 2020).

The combined effects of sea-level rise and increasing frequency of extreme climatic events (Chini et al., 2010; Church et al., 2013), require enhancement of the existing coastal defences to minimize the overtopping consequences. Retrofitting structures and use of soft engineered defences are recommended as a potentially effective approach to improve the performance of existing defences and enhance the resilience of coastal defences to wave overtopping. However, there is a knowledge gap on how effective these soft defences perform when deployed as retrofitting structures in front of an existing defence. Also, a lack of robust predictive relations to evaluate the performance of retrofitting structures in mitigating wave overtopping, has limited the use of these solutions. This paper presents a comprehensive investigation on the performance of four prototype coastal retrofit structures in front of a vertical seawall. The wave overtopping from the retrofitting structures is investigated based on number of physical modelling experiments with a range of hydrodynamic and structural configurations. The outcomes of this study provide new insights and knowledge into how these physical configurations perform, as well as what is the impact of such complex geometries in attenuating the wave overtopping volume from existing vertical seawalls. This paper sets out new robust predictive relations to evaluate the performance of retrofitting structures and predict the wave overtopping from vertical seawalls enhanced with retrofitting.

2. Previous work

Overtopping discharge from vertical seawall

The mean wave overtopping discharge is widely used as a key indicator to evaluate hazardous effects of overtopping events. Franco et al. (1995) conducted two-dimensional laboratory measurements on caisson breakwaters and proposed that mean wave overtopping discharge can be estimated as an exponential function of relative freeboard (R_c/H_{m0}):

$$\frac{q}{\sqrt{gH_{m0}^3}} = a \exp\left(-b\frac{R_c}{H_{m0}}\right), \quad [1]$$

where H_{m0} is the significant wave height from spectral analysis, a and b are empirical coefficients and R_c/H_{m0} is relative freeboard. Number of studies have confirmed Franco et al. (1995) findings (Allsop et al., 2005; Besley et al., 1998). However, further discussions were required on the value of the empirical coefficient a and b, as scatters were noticed between measured and predicted overtopping discharges from Eq.1 (Allsop et al., 2005). These scatters highlighted the importance of identifying more accurate and robust predictive relations for overtopping assessment under impulsive and non-impulsive wave conditions.

No clear boundary is available to distinguish impulsive and non-impulsive waves (Allsop et al., 2005; Goda, 2000; van der Meer and Bruce, 2013). In order to provide classifications between impulsive and non-impulsive conditions, EurOtop (2018) suggests an impulsiveness parameter, h_* ($= \frac{h_s}{H_{m0}}\frac{2\pi h_s}{gT_{m-1,0}^2}$), where h_s is the water depth at the toe of the structure. Wave conditions with $h* < 0.23$ are defined as

impulsive, which are dominated by breaking waves. Conversely, the wave conditions with $h* > 0.23$ are categorized as non-impulsive, where the majority of waves do not break.

For the cases with low relative freeboard, similar mean overtopping discharges were measured for both impulsive and non-impulsive wave conditions. As freeboard increases, impulsive overtopping discharges gradually becomes significantly larger than the non-impulsive overtopping (Allsop, 1995; Besley et al., 1998). For the cases with large relative freeboard, EurOtop (2018) describe the mean overtopping discharge as Eq.2:

$$\frac{q}{{h_*}^2\sqrt{g{h_s}^3}} = a(h_* \frac{R_c}{H_{m0}})^b \quad [2]$$

Although laboratory measurements confirmed that Eq. 2 provides good predictions for impulsive overtopping discharge, significant scatters for cases with small or zero relative freeboard exist, as the overtopping prediction from Eq.2 tend towards infinity. van der Meer and Bruce (2013) proposed improved equations for prediction of non-impulsive (Eq.3) and impulsive (Eq.4 and 5) wave overtopping by adopting exponential functions for those conditions with low relative freeboard. The unified axes in Eq. 3 (non-impulsive) and Eq. 4-5 (impulsive) enable direct comparison between impulsive and non-impulsive conditions. van der Meer and Bruce (2013) modified equations describe impulsive dimensionless discharges as a function of dimensionless freeboard and wave steepness.

$$\frac{q}{\sqrt{gH_{m0}^3}} = 0.05 \exp\left(-2.78 \frac{R_c}{H_{m0}}\right) \quad [3]$$

$$\frac{q}{\sqrt{gH_{m0}^3}} = 0.011 \left(\frac{H_{m0}}{\mathrm{h_s} \cdot \mathrm{s_{m-1,0}}}\right)^{0.5} \exp\left(-2.2 \frac{R_c}{H_{m0}}\right) \quad \text{for } \frac{R_c}{H_{m0}} < 1.35 \quad [4]$$

$$\frac{q}{\sqrt{gH_{m0}^3}} = 0.0014 \left(\frac{H_{mo}}{\mathrm{h_s} \cdot \mathrm{s_{m-1,0}}}\right)^{0.5} \left(\frac{R_c}{H_{m0}}\right)^{-3} \quad \text{for } \frac{R_c}{H_{m0}} > 1.35 \quad [5]$$

where R_c is the crest freeboard of structure, h is the water depth at the toe of structure and $s_{m-1.0}$ is statistical wave steepness.

Although previous studies have focused more on evaluating mean overtopping discharges from coastal structures, in recent years, research emphasis has shift towards understanding the maximum overtopping discharge (V_{max}) during extreme climatic events (Bruce et al., 2001; Pearson et al., 2002; US Army Corps of Engineers, 2008). V_{max} indicates the intensity of overtopping events in a short period, and represents the hazardous impacts of extreme overtopping event. In this study, the V_{max} is determined according to Basley (1998) findings, as a logarithmic function of number of overtopping events, the scale and shape factor (Eq. 6):

$$V_{max} = a(\ln \mathrm{N_{ow}})^{1/b} \quad [6]$$

where V_{max} is maximum individual overtopping discharge per structure width, N_{ow} is the number of overtopping events, a and b are the scale and shape factor, respectively.

EurOtop (2018) proposed empirical relations for estimating N_{ow} for both non-impulsive (Eq. 7) and impulsive (Eq. 8) conditions.

$$\frac{\mathrm{N_{ow}}}{N_w} = exp\left[-1.21\left(\frac{R_c}{H_{mo}}\right)^2\right] \quad [7]$$

$$\frac{\mathrm{N_{ow}}}{N_w} = max\begin{cases} exp\left[-1.21\left(\frac{R_c}{H_{mo}}\right)^2\right] \\ 0.024\left(\frac{{\mathrm{h_s}}^2}{H_{m0}L_{m-1,0}}\frac{R_c}{H_{mo}}\right)^{-1} \end{cases} \quad [8]$$

where N_w is number of incident waves.

Determining the scale and shape factor in Eq. 6 is a challenging task. Parameters *a* and *b* in Eq. 6 are further elaborated according to the wave impulsiveness (Eq. 7 and 8). Eq. 9 describes the scale factor for both impulsive and non-impulsive waves. Eq. 10 and 11 define the shape factor for non-impulsive and impulsive wave conditions, respectively.

$$a = \left(\frac{1}{\Gamma\left(1+\frac{1}{b}\right)}\right)\left(\frac{qT_m}{P_{ov}}\right) \quad [9]$$

where Γ is the gamma function.

$$b = \begin{cases} 0.66 & \text{for } \mathrm{s_{m-1,0}} = 0.02 \\ 0.88 & \text{for } \mathrm{s_{m-1,0}} = 0.04 \end{cases} \quad for \quad {\mathrm{h_s}}^2/\mathrm{H_{m0}}.\mathrm{L_{m-1,0}} > 0.23 \quad [10]$$

$$b = 0.85 \quad \text{for } {\mathrm{h_s}}^2/\mathrm{H_{m0}L_{m-1,0}} < 0.23 \quad [11]$$

The predictive formulae described in this section enable engineers and scientists to estimate mean overtopping discharges from plain vertical seawalls. To date, very limited data and guidance is given for evaluating the influence of additional retrofit structures on overtopping characteristics from vertical seawalls. Hence, considering long-term effects of sea-level-rise, more frequent incidence of extreme climatic conditions and aging of coastal protection infrastructures, it is vital to understand the impacts of additional retrofitting structures on the performance of seawalls in mitigation of mean and extreme wave overtopping.

Effects of recurve wall on overtopping

Kortenhaus et al. (2003) investigated the performance of recurve walls with specific attention to the breaking wave conditions and reported that a reduction in overtopping volume is related to recurve dimensions (Eq. 12 -14).

$$k = \begin{cases} 1.0 & \mathrm{R_c/H_s} \le \mathrm{R_0}^* \\ 1 - \frac{1}{m}\left(\frac{R_c}{H_s} - {R_0}^*\right) & \mathrm{R_0}^* < \mathrm{R_c/H_s} \le \mathrm{R_0}^* + \mathrm{m}^* \\ k_{23} - 0.01\left(\frac{R_c}{H_s} - {R_0}^* - m^*\right) & \mathrm{R_c/H_s} \ge \mathrm{R_0}^* + \mathrm{m}^* \end{cases} \quad [12]$$

$$\mathrm{R_0}^* \equiv 0.25\frac{h_r}{B_r} + 0.05\frac{P_c}{R_c} \quad [13]$$

$$\mathrm{m} \equiv 1.1\sqrt{\frac{h_r}{B_r}} + 0.2\frac{P_c}{R_c} \qquad m^* \equiv m(1 - k_{23}) \quad [14]$$

where P_c and h_r denote the distance from the bottom of recurve to still water level (SWL) and the height of recurve, respectively. B_r is the overhang length of recurve and k_{23} is the lowest *k*-factor (set to 0.20). Despite Eq. 12-14 providing good predictions for the cases with large crest to depth ratio, for most conditions they result in overestimation. Pearson et al. (2004) improved prediction accuracy for recurve walls with use of correction factors (Eq. 15), however, variations between measurements and the revised predictions are still noticeable.

$$k = \begin{cases} k & R_c/h_s \le 0.6 \\ k \times 180\exp\left(-8.5\frac{R_c}{h_s}\right) & 0.6 < R_c/h_s \le 1.1 \\ k \times 0.02 & 1.1 < R_c/h_s \end{cases} \quad [15]$$

where k is given in Eq. 12 by Kortenhaus et al. (2002).

Kortenhaus et al. (2002) and Pearson et al. (2004) data demonstrated that for the cases with low relative freeboard, recurve cannot play a significant role on wave overtopping reduction, whilst for the relative freeboard greater than 1.5, the role of recurve structure in mitigating overtopping becomes significant. Van Doorslaer and De Rouck (2011) studied the effects of recurve geometry on the overtopping mitigation and recommended that angles ≤ 45° is more desirable for structure's stability and improved performance in mitigating overtopping.

Effects of vegetation on overtopping

In recent years, 'green infrastructure' have more extensively been used to improve the resilience of coastal regions, instead of traditional 'hard' coastal defences such as rock walls, armoured wall or embankments. The hard engineered solutions are at increasing threat of structural failure and erosion by extreme events and the sea-level-rise. Unlike hard defences which cannot adapt to the long term impacts of climate change, the soft nature-based solutions are capable of adapting to climate change consequences. The 'self-healing' ability of soft defences make them promising cost effective and efficient coastal defence solutions. However, there is significant gap of knowledge in how soft retrofitting solutions perform in terms of wave overtopping mitigation. Lack of guideline on overtopping estimation from soft defences has limit the use of such solutions and there is need for more comprehensive research and data to understand overtopping processes from soft defences as well as providing predictive relations for overtopping from these retrofits.

Recent studies (Kobayashi et al., 2013; Feagin et al., 2019; Bryant et al., 2019) show that vegetation is capable of attenuating wave run-up and overtopping through dissipating wave turbulent kinetic energy. Luhar et al. (2017) investigated the effects of seagrass meadow on wave turbulence decay through physical modelling experiments and suggested that stem density and submergence depth of seagrass impact the wave amplitude reduction. Also, it was found that impacts of seagrass on wave energy dissipation varies with incident wave kinematics including wave period T and wave height H_s. Luhar et al. (2017) results indicate that higher wave velocities are associated with more efficient behaviour of seagrass resulting in greater wave energy dissipations. Experimental investigations show a reduction of up to 40% in the wave amplitude due to seagrass drag effects.

Maza Fernandez et al. (2017) investigated the impact of mangrove forest in reduction of wave velocity due to complex and porous nature of mangrove's roots. It was shown that the drag effects of individual trunk near the bed and the frontal area at the top of root contribute to up to 50% reductions in wave velocity. Field-based measurements conducted by Tanaka et al. (2007) and Forbes and Broadhead (2007) from the Indian Ocean 2004 tsunami in, illustrated that areas with higher density vegetation in coastal regions usually had suffered less damage. Additionally, it was found that for similar vegetation density, the protection provided varies with vegetation shapes. Tanaka et al. (2007) data showed that mangroves were efficient in mitigating tsunami waves when the density exceeded 14 – 26 elements per 100 m^2, while coconut trees did not show any effective performance in mitigating tsunami waves regardless of their density. Findings of Tanaka et al. (2007) could be associated with the complex root structure of mangroves which maximize wave-structure interactions and therefore dissipate wave energy more significantly in comparison to coconut trees. To this date, very limited research has been conducted to understand the impact of vegetation configurations (or any other 'soft defences') on the reduction of wave overtopping.

Very little research into the performance of diffraction pillars and reef breakwater, as retrofitting structures, is available, and therefore no robust evidence on wave overtopping reduction capabilities is available. Physical modelling experiments are needed to study the effects of these two retrofitting structures on the foreshore of coastal defences.

The literature shows, very limited research has been conducted to understand the performance of retrofitting structures (both hard and soft retrofits) and the role they can play in mitigating wave overtopping from vertical seawalls. This paper presents laboratory-scale physical modelling study of four types of retrofitting structures when placed in front of a plain vertical seawall. Detailed wave conditions are designed to investigate the impact of these retrofitting structures on enhancing resilience of the seawall and wave overtopping reduction during swell and storm conditions. Furthermore, this study proposed robust predictive relations for evaluating wave overtopping discharge from the retrofitting structures.

3. Physical Modelling Experiments

A comprehensive set of physical modelling study was undertaken in Warwick Water Laboratory to investigate the performance of four prototype retrofitting structures in mitigating wave overtopping, when placed in front of a vertical seawall. The tests were performed in a wave flume of 22m (l) × 0.6m (w) × 1m (h) with a 1:20 smooth impermeable beach slope (Fig. 1). The flume was equipped with a piston-type wave generator with an active absorption system. Experiments were carried out with vertical seawall fixed at 12.2m from the wave-maker paddle (Fig. 1).

Each test case was consisted of approximately 1000 pseudo-random waves based on the JONSWAP spectrum with peak enhancement factor γ= 1.0 (i.e. Pearson and Moskowitz). The characteristics of incident waves and free-surface elevations were determined using six wave gauges across the flume (see Fig. 1). Three wave gauges were setup close to the paddle and three in front of the seawall, the distance between the gauges was determined based on the Least-Square Method described by Mansard and Funke (1980).

The overtopping volumes were measured by a system of collection tank and load-cell which was placed behind the vertical seawall. The load-cell was setup to measure wave-by-wave overtopping volume. An overtopping detector circuit was installed on the crest of seawall to record the temporal distribution of individual overtopping events. A syphon mechanism was fixed over the container to ensure continuous sampling for the duration of the test.

The investigations include both soft and impermeable hard retrofit prototypes to understand their impacts on mitigating wave overtopping from vertical seawalls. Four coastal retrofits including, diffraction pillars, reef breakwaters, recurve wall and vegetation were investigated (Fig. 2). For each test configuration, the retrofit element was installed at approximately 0.5m from the seawall.

Table 1 summarizes the experimental setup and wave conditions for the physical modelling tests conducted within this study. Two seawall prototypes with varying heights were used for tests with both impulsive and non-impulsive conditions, covering a comprehensive range of dimensionless freeboard R_c/H_{m0}. The significant wave height ranged from 0.047 – 0.14m, and four wave period of T_p = 1.25, 1.50, 1.75 and 2.0s were tested for each set of experiment. All experimental scenarios were tested with still water depth h_s = 0.07, 0.1 and 0.13m at the seawall. The wave conditions tested in this study were designed to cover a range of wave steepness S_{op} between 0.016 - 0.06.

4. Results and Discussion

4.1 Validations of reference cases

Incident wave characteristics have been studied comprehensively by researchers (Longuet-Higgins, 1952; Battjes and Groenendijk, 2000; Goda, 2010). For waves generated based on JONSWAP spectra, Longuet-Higgins (1952) found that individual wave height in deep water follows the Rayleigh

distribution. As the waves move to shallower water, the incident waves become unstable and break, resulting in gradual deviation of wave height from the Rayleigh distribution (EurOtop, 2018).

The wave conditions are validated by determining the wave height distribution for all the test cases. Fig. 3 presents the wave height distribution in deep water (near wave paddle) for the two seawall prototypes tested in this study. The wave characteristics for Fig. 3a & 3b are described in the figure caption. Figs.3a & 3b indicate that the measured wave heights are in good agreement with the Rayleigh distribution, with a RMSE of 0.099 and 0.152, respectively. However, some scatter is observed for the largest waves which represents extreme events (Fig. 3b). The deviations from Rayleigh distribution occur due to high wave steepness (S_{op}) of large individual waves, which break close to paddle, rather than shallow water column of the surfzone.

The distribution of individual overtopping volume on plain vertical seawall (used as reference case) is investigated and the results are compared against empirical relations proposed by EurOtop (2018). Previous work show that the individual wave overtopping volume follows a two-parameter Weibull distribution (Pearson et al., 2002; Victor et al., 2012; Zanuttigh et al., 2013). Fig. 4 shows distribution of wave by wave overtopping volume measured for two of the wave conditions tested within this study and confirms that exceedance probability follows the Weibull relationship for individual overtopping volumes. For extreme scenarios with large overtopping volumes, limited scatters from Weibull distribution are evident in Fig. 4.

The Weibull plots of individual overtopping volume can be further analysed to determine the Weibull *b* parameter (shape parameter in Eq.6) for predicting the maximum overtopping volumes. Previous studies highlighted the changes in the behaviour of Weibull distribution when '*b*' parameter is fitted with either upper or lower parts of individual overtopping volumes (Formentin and Zanuttigh, 2019b; Molines et al., 2019b). It was found that fitting the shape parameter *b* using the highest 10% volumes provides better estimations of the maximum individual overtopping volume, compared to that of highest 50% volumes (Hughes et al., 2012; Zanuttigh et al., 2013). Following the procedures recommended by Pearson et al. (2002), the Weibull's *b* parameter was determined as the gradient of linear regression line of individual overtopping volumes.

The mean overtopping discharges from plain vertical walls are compared to the empirical predictions proposed by EurOtop (2018) [Eq. 3-5]. The laboratory measurements are in good agreement with the empirical relationships (Fig. 5). However, the largest scatter is observed for the cases with $R_c/H_{m0} \approx 2.2$, where the physical modelling measurements are a factor of two smaller than empirical predictions. The deviations in mean overtopping discharge from EurOtop (2018) predictions are due to differences in the peak enhancement factor of the JONSWAP spectrum implemented in this study (γ=1.0) and the EurOtop (γ= 3.3). The peak enhancement factor γ, specifies the peak energy of the wave spectrum, and this study focuses on relatively lower γ (=1.0) for the physical modelling experiments.

4.2 Overtopping measurements from retrofits

Overtopping discharges

The performance of proposed retrofitting prototypes is evaluated by comparing the mean overtopping discharges to the overtopping measured for the plain vertical seawall (reference case). Fig. 6 and 7 compares the measured mean overtopping discharge between reference cases and the retrofit structures for impulsive and non-impulsive wave conditions, respectively. The results illustrated in Fig. 6 indicate that the reduction in mean overtopping discharges for the retrofits varies with dimensionless freeboard (R_c/H_{m0}). For the retrofitting cases with larger relative freeboards, a higher reduction in mean overtopping discharges is observed. For the R_c/H_{m0} larger than 2.25, recurve walls provide the maximum reduction of mean overtopping discharge (98% reduction), followed by model vegetation with 93% and reef breakwater with 88% reduction. The minimum reduction in mean overtopping discharges were detected when the dimensionless freeboard was less than 1.0, where a 63% reduction in mean discharge was observed for the recurve wall, followed by vegetation (61%) and reef breakwater (59%). The diffraction pillars did not show significant efficiency for the test cases with dimensionless freeboard less than 1.0, with maximum of 6% overtopping reduction over all wave conditions.

Overtopping Proportion

In addition to the mean overtopping discharge, retrofitting structures will also influence overtopping proportion. The proportion of overtopping waves can be described by a Weibull distribution (EurOtop, 2018). The measurements from this study (P_{ov}) are compared to the predictions described by EurOtop (2018) using the recommended $h_s^2/H_{m0}L_{m-1,0}$ values (Fig. 8). Fig. 8 shows that recurve wall performs as the most efficient retrofit in reducing wave overtopping proportion, amongst the four prototypes investigated in this study. The performance of recurve wall becomes more significant as R_c/H_{m0} increases, the results show the overtopping proportion decreases by half for $R_c/H_{m0} = 1.0$, while over 85% reduction is observed when R_c/H_{m0} is greater than 2.3. Fig. 8 indicates that the vegetation retrofit also provides significant reduction in overtopping proportion, with over 80% reduction in P_{ov} for the cases with $R_c/H_{m0} >$ 2.3. However, for the cases with low relative freeboards, no significant reduction in P_{ov} was measured for the vegetation. The measurements show that reef breakwater and diffraction pillars are not significantly reducing P_{ov}, with an average of 30% and 10% reductions in P_{ov}, respectively.

Extreme overtopping events

The mean overtopping discharge and overtopping proportion is by definition described by the performance of retrofitting structures in a time-averaged concept. A comprehensive evaluation of overtopping needs understanding of the intensity of waves as well as wave-by-wave overtopping events, highlighting the potential threat to people and critical infrastructures originated from these potentially hazardous events. In this study, the maximum individual overtopping discharge is used to evaluate the performance of retrofitting structures to instantaneous overtopping events. Fig. 9 shows the comparison

between the measured maximum individual overtopping volumes with the empirical prediction given by EurOtop (2018). For the case of plain vertical wall, good agreement exists between the experimental data and empirical predictions (Eq. 6 - 11). The measurements show that model vegetation is the most efficient retrofitting in mitigating V_{max}, with a minimum reduction of wave-by-wave overtopping of 48%, followed by reef breakwater (30%) and recurve wall (28%). In addition, for the large and small individual overtopping events, the measurements of V_{max} show a diverse performance for the retrofitting structures. More significant reductions are observed in small overtopping events. The measurements show that for V_{max} of ~5×10^{-3} (m^3/m), the maximum reduction of V_{max} is approximately at a factor of 4, while more than one order of magnitude reduction is observed for the cases of V_{max} less than 2×10^{-4} (m^3/m).

4.3 Influences of Structural Dimensions on Wave Overtopping

Despite the dominant effects of freeboard on the performance of retrofitting structures, the overtopping is also influenced by geometrical shape of the structure. Changes in the shape of retrofitting can alter water depth at the of toe of the structure, freeboard height and overall roughness of the structure, which can affect the overtopping results. This section will investigate the impacts of geometrical dimension changes on the wave overtopping mitigating effects of retrofitting structures.

Reef breakwater

Analysis of overtopping events indicate that performance of reef breakwater is directly influenced by submergence depth (water depth above the breakwater crest). The measurements show that limited submergence depth lead into inefficiency of reef breakwater and in some cases (e.g., $R_c/H_{m0} \approx 2.25$), wave overtopping discharge are larger than those recorded for the reference case (highlighted by circle in Fig. 7). Besley et al. (1998) reported similar overtopping characteristics with field measurement data from the coast of Samphire, Hoe. Increases in wave overtopping discharge are caused by complex interactions between the relatively low wave height and water depth above the crest of reef breakwater, which increase wave 'tripping' onto the foreshore berm, and intensify overtopping discharges (Allsop et al., 2003; Allsop et al., 2005). The increase in overtopping for the case of reef breakwater retrofitting is due to the sudden reduction of water depth at the breakwater which leads to reef induced wave breaking process in front of the seawall (Johnson, 2006; Xu et al., 2020; Yao et al., 2013). The rapid wave transformations from non-breaking condition on the foreshore of the reef to breaking at lee-side of breakwater, quickly fill the gap between the retrofit and seawall, leading to an increase the local mean water depth in front of the seawall. This locally elevated mean water depth allow the incident waves to roll on top of the previous broken wave envelope due to the interactions with the reef, filling the available freeboard in front of the seawall which can make the seawall more prone to wave overtopping.

Despite this study highlights the water depth and wave conditions threshold for intensified overtopping phenomena, further investigations with a range of freeboards between 1 to 3 are required for more comprehensive evaluation of reef breakwater performance.

Vegetation

The performance of model vegetation in mitigating overtopping volume is predominantly influenced by the packing density and width of the vegetation. Previous research studied influences of packing density in wave turbulent kinetic energy decay (Luhar et al., 2017; MacArthur et al., 2019). However, the influence of packing density on wave overtopping mitigation has not been investigated to date. This study used four packing densities for the model vegetation retrofit which were built with flexible straws. Straws were sealed on a PVC board, with dimensions of 600 × 600 mm. The PVC board was sealed in front of the seawall to hold straws in place. Fig. 10 shows the schematics of straw configurations for the four packing density of 0.04 stems/100mm^2, 0.17 stems/100mm^2, 0.33 stems/100mm^2 and 0.5 stems/100mm^2. If the packing densities tested within this study are converted into field scale, they are equivalent of 19 stems/100m^2, 75 stems/100m^2, 133 stems/100m^2 and 200 stems/100m^2, respectively. The packing densities used for the physical modelling were derived based on previous work on the performance of coastal wetland vegetation (100 – 600 stem/m^2) on damping wave energy (Augustin et al. (2009), coconut trees (14 – 26 stems/100m^2) and dense mangroves (10 – 20 stems/100m^2) against tsunami (Forbes and Broadhead, 2007; Tusinski and Verhagen, 2014).

Measurements show that increased packing density led to larger reduction in wave overtopping (Fig. 11). When packing density increases from 19 to 200 stems/100m^2, the mean overtopping discharge behind the seawall decreases, in average, by a factor of 3. The performance of model vegetation is also affected by freeboard. For the packing density of 19 stems/100m^2, the reduction in overtopping discharge γ rises from 28% for the case of freeboard = 0.95 to 72% for the freeboard of 2.33. For the packing density of 200 stems/100m^2, the mean overtopping discharge decreases by two orders of magnitude for relatively small freeboards, while for the larger freeboards the reduction in overtopping reaches the maximum at three order of magnitude. The performance of model vegetations with regards to packing density and dimensionless freeboard is further investigated. Fig. 12 and 13 show the wave overtopping reduction γ against packing density of vegetation and dimensionless freeboard, respectively. The reduction γ increases exponentially with increase of packing densities. Increasing packing density from19 stems/100m^2 to 200 stems/100m^2 led to an average increase in γ from 45% to 99% (Fig. 12). The measurements show that there is a sharp improvement in the performance of model vegetation when transitioning from lower packing density to higher packing density, while there is no major changes in the performance of the vegetation when the packing density is increased from a relatively higher densities. The reduction in overtopping discharge is increased by 30% on average, when packing density rise from 19 stems/100m^2 to 75 stems/100m^2. However, only 20% improvements are observed in overtopping reduction when density increases from 75 stems/100m^2 to 200 stems/100m^2.

Fig. 13 shows the relationship between dimensionless freeboard and reduction in overtopping discharge γ for the four packing density tested within this study. It is evident that increase in dimensionless freeboard significantly improve the performance of vegetation. For the cases with a high packing density (200stems/100m^2), regardless of the freeboard, model vegetation is proven to be efficient in attenuating wave overtopping discharge.

The effects of packing density on the individual overtopping events is investigated in Fig. 14. The results illustrate that the V_{max} decreases with increasing packing density of vegetation, the maximum V_{max} reduction of two orders of magnitude was recorded for the packing density of 200 stems/100m^2. The measurements show that for each packing density scenario, the mitigation in V_{max} are nearly constant for both large and small maximum individual overtopping events.

Comparison of V_{max} from different packing densities indicates the higher packing density lead into smaller V_{max}. Increasing packing density from 75 to 133 stems/100m^2, led into V_{max} reduction rises from a factor of ten to two orders of magnitude. It is also found that the performance of vegetation in reducing V_{max} does not linearly increases with the packing density. The higher packing density, the more significantly V_{max} is attenuated.

Recurve wall

Previous work on influence of recurve dimension on the performance of recurve walls have highlighted the significance of overhang length and height of recurve. Kortenhaus et al. (2003) and Pearson et al. (2004) developed predictive formulae for overtopping discharges on recurve walls according to their overhang length and height. Although these equations provide insight on the performance of recurves, but given that they don't consider the influences from wave characteristics on the performance of recurve, scatters between these equations and experimental results for cases with the same structural dimensions can occur.

Fig. 15 - 16 summarize the overtopping discharges measured from recurve wall under impulsive and non-impulsive conditions, respectively. The results show that both impulsive and non-impulsive overtopping measurements on the recurve wall follow a similar trend to those equations used in the reference cases. Under impulsive conditions, recurve wall can reduce mean overtopping at a maximum of two order of magnitude, demonstrating a strong performance in mitigating wave overtopping. The reduction in mean overtopping discharge increases with R_c/H_{m0}, but it remains approximately constant when $R_c/H_{m0} > 2.5$ (Fig. 15). For the non-impulsive conditions, the previous work concluded that, incident waves fill the gap area under the recurve very quickly and therefore the recurve cannot perform very efficiently in reducing overtopping volume (Kortenhaus et al., 2003; Pearson et al., 2004). However, for the configurations tested within this study, recurve wall offers satisfactory reduction in the mean overtopping discharges for non-impulsive conditions (Fig. 16). It is noticeable that recurve wall decreases the overtopping discharge up to an order of magnitude, and no overtopping events were observed for tests with dimensionless freeboard greater than 2.5.

Kortenhaus et al. (2002) and Pearson et al. (2004) proposed that the overtopping discharge reduction from recurves can be predicted as a function of recurve dimensions. Fig. 17 compares the total overtopping volume measured from recurve wall with predictions obtained from Kortenhaus et al. (2003) and Pearson et al. (2004) methodology. Satisfactory agreement was observed between the measured and predicted overtopping discharge when $R_c/h_s \approx 1$. For $R_c/h_s > 1.5$, the deviation between measured and predicted values are increased and predictive relations overestimate the overtopping reduction by an order of magnitude. In Fig. 17, a range of overtopping discharges are noticeable for the same R_c/h_s. The deviations between results with the same R_c/h_s can be over a factor of 10, and they are believed to be caused by low wave steepness in tested conditions, which showed more likelihood to overtop at the seawall.

Overtopping discharge reduction on retrofitting structures

To compare the effectiveness of retrofits, reductions in mean overtopping discharge were analysed for all configurations. Reduction γ is calculated as the ratio of decreased discharge over the measured discharges from the reference case. Fig. 18 shows how the mean overtopping discharge is decreased by retrofitting structures. Amongst the four retrofits tested in this study, the best performance in mitigating mean overtopping discharge was observed for recurve wall followed by model vegetation. Diffraction pillars reduced the mean overtopping discharge for the cases with relatively large dimensionless freeboard but offered limited contributions on reducing mean overtopping discharge for the cases with low dimensionless freeboard.

Fig. 18 confirms that a larger dimensionless freeboard improves the performance of retrofitting in mitigating mean overtopping discharges. For the cases with low freeboards ($R_c/H_{m0} < 1.3$), the recurve wall provides the best performance with 78% average mean overtopping discharge reduction, followed by the vegetation and reef breakwater with 73% and 72% average discharge reduction, respectively. The diffraction pillars did not prove to be as efficient, with a 38% reduction in overtopping discharge for $R_c/H_{m0} < 1.3$. Increases in the relative freeboard resulted in improved overtopping reduction performance of all the retrofitting structures. For the test cases with $1.3 < R_c/H_{m0} < 3.0$, the mean overtopping discharge reduction increased from 38% to 78% for the diffraction pillars and for other three retrofitting configuration, the overtopping discharge reduction increased up to 99%. For the cases with $3.0 < R_c/H_{m0} < 3.8$, the reduction in mean overtopping discharge on all retrofitting structures became approximately constant (99% for recurve wall, 98% for reef breakwater, 88% for vegetation and 78% for diffraction pillars), and no overtopping events are observed for recurve wall when $h_* > 0.065$.

Besides the relative freeboard, wave impulsiveness is also a key parameter which can significantly affect the wave-structure interactions (Kisacik et al., 2012; Oumeraci et al., 1993; Ravindar et al., 2019), and influence the performance of retrofitting structures in mitigating mean overtopping discharge. The highlighted data in Fig. 18 (red dotted line), show the extreme low discharge reduction (of approximately

20%) compared with measurements from other conditions with similar R_c/H_{m0} (with approximately 80% reduction). Reviewing the wave conditions for the cases highlighted in Fig. 18 show that the wave impulsiveness for these highlighted cases are around 0.015, while the wave impulsiveness for other cases with similar R_c/H_{m0} is approximately 0.03. Hence, the results indicate that low wave impulsiveness is the underlying reason for very small mean overtopping discharge mitigation from diffraction pillars (highlighted cases in Fig. 18).

Fig. 19 highlights the combined influence of wave impulsiveness h_* and relative freeboard R_c/H_{m0} on the mean overtopping reduction γ on retrofitting structures. In general, the reduction (γ) in the mean overtopping discharge is directly influenced by $h_* \times R_c/H_{m0}$. For the cases with $0.15 < h_* \times R_c/H_{m0} < 0.25$, the data shows a constant reduction in mean overtopping discharge with the minimum of 82% on all tested retrofitting structures. When $h_* \times R_c/H_{m0}$ decreases and approaches towards zero, the γ sharply reduces. Further analysis of data showed that for all $h_* \times R_c/H_{m0}$ conditions tested in this study, recurve wall is found to be the most effective retrofitting structures, while the diffraction pillars are the least efficient (5% reduction in mean overtopping) mainly for the test conditions with small freeboard and low wave impulsiveness ($h_* \times R_c/H_{m0} < 0.05$).

The analysis of results discussed in Fig. 18 and 19 indicate that, the relative freeboard is the dominant factor in reducing mean overtopping discharge from retrofitting structures. For the cases with small relative freeboard, the wave impulsiveness plays a key role in determining the performance of retrofitting structure in mitigating wave overtopping discharge.

Further analysis on structural height and water depth at the toe of the structures is undertaken to understand the influence of retrofitting's structural dimensions on mitigating mean wave overtopping discharge. Fig. 20 illustrates the relationship between mean overtopping discharge reduction and dimensionless area of retrofitting structures. The cross-sectional area of retrofitting structures is non-dimensonalised by cross sectional area of water body (width of the flume multiplies water depth at the toe of seawall). Fig. 20 only analyses the retrofits which were placed on the foreshore beach slope of the flume (excluding recurve wall). The results presented in Fig. 20 highlight that the overtopping reduction increases with dimensionless area and when the dimensionless area approaching zero, the overtopping reduction falls sharply. A significant deviation from the overall trend of data in Fig. 20 can be seen in one data point at $R_c/H_{m0}=3.0$, which can be attributed to high wave impulsiveness ($h_*<0.02$) for this case.

4.5 Prediction of overtopping discharges from retrofits

Reliable predictive tools for understanding the performance of retrofitting structures are key for coastal engineers and planners, enabling assessment of safety level behind coastal defences. The laboratory measurements of overtopping discharges from the retrofitting prototypes tested within this study are adopted for deriving empirical-based predictive tools. Previous research (described in §2) suggest, for cases with high relative freeboard, the mean overtopping discharge can be predicted as power law

function of freeboard, while for those cases with small or zero freeboard, the overtopping can be estimated by exponential function of the freeboard (EurOtop 2018). Eq. 3 – 5 are recommended by EurOtop (2018) are the most widely used relations to evaluate the overtopping discharge as function of relative freeboard. In this project, Eq. 3 - 5 are adopted for two relative freeboard regimes of R_c/H_{m0} < 1.35 and R_c/H_{m0} > 1.35, to fit overtopping discharge measurements from retrofitting structures tested within this study.

The $H_{m0}/h\times s_{m-1,0}$, in EurOtop (2018) predictive formulae (Eq. 4 and 5), varies across cases due to different wave characteristics including H_{m0} and $T_{m-1,0}$. To simplify empirical-based regression equations, this study adopts an average of tested $H_{m0}/h\times s_{m-1,0}$ for each test configuration.

Statistical analysis was carried out to evaluate the performance of regression equations developed in this study. The root-mean-square error (RMSE) was calculated according to Eq. 16, to determine deviations of proposed regression equations from laboratory measurements.

$$\mathrm{RMSE} = \sqrt{\frac{\sum_{i=1}^{n}(\log_{10} y_i - \log_{10} \hat{y}_i)^2}{n}} \qquad [16]$$

where n is the total number of data points used for analysis, the subscript i is the number of data points, y_i denotes the observation for i^{th} data point and the $\hat{y}_i$ represents the predicted value for i^{th} data point from regression equations. The measured mean overtopping discharges on the plain vertical seawall were compared with the prediction formulae from the EurOtop (2018), and an RMSE=0.60 was obtained. Further analysis of data recorded for the reef breakwater retrofit was conducted to find out the best empirical-based predictive relations for overtopping from both impulsive and non-impulsive wave conditions. The best-fit relations for impulsive wave conditions are described in Eq. 17, where two equations are suggested based on relative freeboard ($\frac{R_c}{H_{m0}}$):

$$\begin{aligned} \frac{q}{\sqrt{gH_{m0}^3}} &= 0.0055 \times \left(\frac{H_{m0}}{\mathrm{h}_s \times S_{m-1,0}}\right) \exp\left(-3.15\frac{R_c}{H_{m0}}\right) \qquad \text{for } \frac{R_c}{H_{m0}} < 1.35 \\ \frac{q}{\sqrt{gH_{m0}^3}} &= 0.0002 \times \left(\frac{H_{m0}}{\mathrm{h}_s \times S_{m-1,0}}\right) \left(\frac{R_c}{H_{m0}}\right)^{-3.1} \qquad \text{for } \frac{R_c}{H_{m0}} > 1.35 \end{aligned} \qquad [17]$$

The statistical measures (RMSE = 0.524 and R^2=0.86) show that the proposed predictive relations are in good agreement with the physical modelling measurements.

The laboratory measurements for the case of diffraction pillar was employed for deriving empirical regression model. Eq. 18 presents the predictive relations for evaluating wave overtopping from diffraction pillar retrofit under impulsive conditions. The RSME (=0.25) and R^2 (=0.80) shows that the formulae proposed in this study are capable of predicting wave overtopping with acceptable accuracy.

$$\frac{q}{\sqrt{gH_{m0}^3}} = 0.01 \times \left(\frac{H_{m0}}{\mathrm{h}_s \times S_{m-1,0}}\right) \exp\left(-3\frac{R_c}{H_{m0}}\right) \qquad \text{for } \frac{R_c}{H_{m0}} < 1.35 \qquad [18]$$

$$\frac{q}{\sqrt{gH_{m0}^3}} = 0.00046 \times \left(\frac{H_{m0}}{\mathrm{h}_s \times S_{m-1,0}}\right)\left(\frac{R_c}{H_{m0}}\right)^{-3.23} \qquad \text{for } \frac{R_c}{H_{m0}} > 1.35$$

Eq. 19 describe empirical-based predictive relations proposed for evaluating mean overtopping based on laboratory measurements on recurve wall. The statistical measures (RMSE=0.5, R^2=0.78) show that the proposed relationship is in good agreement with the measurements.

$$\begin{aligned} \frac{q}{\sqrt{gH_{m0}^3}} &= 0.0016 \times \left(\frac{H_{m0}}{\mathrm{h}_s \times S_{m-1,0}}\right)\exp\left(-4.5\frac{R_c}{H_{m0}}\right) \qquad \text{for } \frac{R_c}{H_{m0}} < 1.35 \\ \frac{q}{\sqrt{gH_{m0}^3}} &= 0.00011 \times \left(\frac{H_{m0}}{\mathrm{h}_s \times S_{m-1,0}}\right)\left(\frac{R_c}{H_{m0}}\right)^{-3.5} \qquad \text{for } \frac{R_c}{H_{m0}} > 1.35 \end{aligned} \quad [19]$$

Eq. 20 describes mean overtopping predictive relationship for the case of model vegetation retrofit with packing density of 75 stems/ 100m^2. The RMSE for the proposed equations is 0.26 and the R^2=0.70, which confirms Eq. 20 can evaluate overtopping discharge from vegetation retrofit when placed in front of a vertical seawall.

$$\begin{aligned} \frac{q}{\sqrt{gH_{m0}^3}} &= 0.0053 \times \left(\frac{H_{m0}}{\mathrm{h}_s \times S_{m-1,0}}\right)\exp\left(-3.5\frac{R_c}{H_{m0}}\right) \qquad \text{for } \frac{R_c}{H_{m0}} < 1.35 \\ \frac{q}{\sqrt{gH_{m0}^3}} &= 0.00011 \times \left(\frac{H_{m0}}{\mathrm{h}_s \times S_{m-1,0}}\right)\left(\frac{R_c}{H_{m0}}\right)^{-2.78} \qquad \text{for } \frac{R_c}{H_{m0}} > 1.35 \end{aligned} \quad [20]$$

Fig. 21 compares the predictive relations derived for the four retrofitting prototypes tested in this study (Eq. 17 – 20) with the laboratory measurements (§4.1- §4.4). Fig. 21 illustrates that the proposed predictive formulae are capable of robust evaluation of overtopping discharge from the retrofitting structures tested in this study. Table. 2 summarises the statistical measures determined for the proposed predictive formulae. RMSE results show that proposed equations for retrofitting configurations are in well agreement with the measurements.

The empirical-based predictive relations (Eq. 17 – 20) are derived from the physical modelling data using the well-established method of "best-fitting" of the laboratory measurements in accordance with the methodology proposed by EurOtop (2018).

Ideally, the wave overtopping prediction formulae for retrofitting structures should include dimensional characteristics as predictive variables to allow engineers and designers have a better understanding of the impact of their retrofit design on the mean overtopping reductions. Given that our measurements in this study are mostly based on single-size prototypes, effects of different structural geometries (retrofitting structure type) are reflected in Eq. 17-20 by use of empirical coefficients. To incorporate structural dimensions as a variable in predictive relations, with high confidence, further studies with

varying retrofitting dimensions are necessary. Furthermore, additional data for the cases of small to zero relative freeboard are required for additional validation of the proposed predictive relations.

5. Discussions

Coastal defences play vital roles in protecting coastal communities from extreme climatic events and provide resilience to flooding (Abolfathi et al., 2016). Given the climate change projections, sea-level-rise will reduce the freeboard level of existing defences. Meanwhile, more frequent extreme weather condition in the future will increase the overtopping volume from seawalls, which could lead into catastrophic coastal flooding. Hence, it is necessary to enhance the resilience of existing coastal defences with use of effective and sustainable approaches. Retrofitting of existing seawalls is a sustainable and effective method of improving climate and flood resilience of existing seawalls.

This study investigated the performance of four types of retrofitting structures in reducing wave overtopping from a plain vertical seawall. Three retrofitting models including diffraction pillars, reef breakwater and vegetation were installed on the foreshore beach, and recurve wall was installed on the sea-ward crest of the seawall. The retrofitting structures were tested for both swell and storm wave conditions. Despite Kortenhaus et al. (2003) reported that recurve wall does not perform well under non-impulsive conditions, the measurements from physical modelling tests show that recurve wall performs very effectively for both impulsive and non-impulsive wave conditions and return significant proportion of overtopping waves from the vertical seawall. The discrepancies between the data presented in this study and Kortenhaus et al. (2003) can be associated to the lower range of h_r tested by Kortenhaus et al. (2003), as the recurve tested in their study was lower than the crest of seawall. Therefore, it can be interpreted that for Kortenhaus et al. (2003) experimental condition, the gap area under the recurve wall was quickly filled with incident waves, creating a region of high mean-sea-level in front of the seawall and facilitating number of overtopping events. However, in this study a higher range of h_r was tested resulting in lower overtopping.

Overtopping measurements show that longer overhang length can provides larger reduction in the overtopping discharge. Furthermore, the measurements show that recurve wall have better performance for those conditions with higher wave steepness. The deviations are noticeable between the measured reduction in the mean overtopping discharge for recurve wall and those predicted from Kortenhaus et al. (2003) formulae. The existing predictions can be further enhanced by considering the effects of wave steepness in the equation proposed by Kortenhaus et al. (2003).

The laboratory investigations for diffraction pillars and reef breakwater, which was placed on the foreshore of the seawall structure, show that performance of these retrofitting structures is a complex function of structural geometry, cross-sectional area, freeboard and impulsiveness of incident waves. It was shown that limited submergence depth can facilitate extreme overtopping events for reef breakwaters. The limited performance of reef breakwater for low submergence depth is due to sudden and local change in wave steepness and breaker type once the wave reaches the breakwater. The

inefficiency of diffraction pillars in reducing mean wave overtopping discharge from the seawall can be associated with the limited cross-sectional area, structural geometry and the consequent hydrodynamic response of incident waves interacting with the diffraction pillars. Detailed analyses of physical modelling results confirm limited use and efficiency for diffraction pillars as a retrofitting option, highlighting the need for understanding the effects of geometrical shapes on wave-structure interactions. Vegetation is a low-cost sustainable retrofit which can enhance the resilience of existing coastal defences by providing buffer layers which dampen the turbulent energy of the incident waves and therefore mitigate overtopping. This paper investigated the impact of vegetation on foreshore of seawalls. The measurements for both impulsive and non-impulsive wave conditions show that packing density and stiffness factor of vegetation are the key parameters determining how effective vegetation will perform in wave overtopping mitigation. Four packing densities were investigated in this study with the equivalent field-scale densities of 19, 75, 133 and 200 stems/100m^2 to mimic the coastal wetland vegetation (100 – 600 stem/m^2), coconut trees (14 – 26 stems/100m^2) and dense mangroves (10 – 20 stems/100m^2). It was found that the vegetation with the lowest packing density (19 stems/100 m^2) did not reduce the mean overtopping discharge significantly. The performance of vegetation becomes acceptable when the density was raised to 75 stems/100 m^2, which was also found to be the most cost beneficial packing density. If using other types of vegetation with branches at lower level close to the sea floor, lower densities would be recommended.

6. Conclusions

This paper presents a comprehensive set of laboratory investigations to quantify and evaluate the performance of four coastal retrofit structures with distinct geometrical properties, when placed in front of a plain vertical seawall, under the influence of impulsive and non-impulsive wave conditions.

The analysis of laboratory measurements shows that all proposed retrofitting structures are effective in mitigating both mean and wave by wave overtopping events. The recurve wall was proven to be the most efficient retrofitting approach, with 98% reduction in mean overtopping volumes. The reduction up to two order of magnitude is achieved in the mean overtopping discharge, even under non-impulsive wave conditions, demonstrating a strong performance of recurve wall in mitigating wave overtopping. Vegetation and reef breakwater also showed significant impact on mitigating overtopping volume, especially against extreme large overtopping events, with overtopping reduction over 48% and 30%, respectively. The laboratory measurements showed that diffraction pillars did not show significant efficiency in reducing wave overtopping from the seawall with 6% reduction in mean overtopping discharge.

The parametric analyses of the physical modelling results showed the mitigating impacts of all retrofitting structures is influenced by the relative freeboard, wave characteristics and the geometric size of the retrofits. The wave overtopping measurements for all tested retrofitting structures show more effective performance of retrofitting with higher relative freeboard R_c/H_{m0} resulting in lower

overtopping rate. In addition, the wave characteristics and the geometric size of the retrofits also influence the overtopping reduction from retrofitting structures. For the cases with R_c/H_{m0}<2.5, the increase in wave impulsiveness (h_*) and cross-sectional area of retrofitting structures led into greater reduction in the mean overtopping discharges.

The effectiveness of model vegetation retrofit is also significantly affected by its pecking density. As packing density increases from 19 stems/ 100m2 to 200 stems/ 100m2, the reduction in all performance indicators increases sharply (e.g., the mean overtopping discharges, maximum overtopping volumes). The measurements show reduction in both mean and maximum overtopping discharges, increases up to five folds as packing density increases.

For the wave overtopping from retrofitting configurations, this study highlights: i) recurve retrofit is a very effective in reducing the overtopping volume under both impulsive and non-impulsive wave conditions. ii) the relative freeboard and overtopping rate are key parameters determining the performance of retrofitting structures. iii) effectiveness of vegetation as a retrofitting solution for mitigating wave overtopping is highly dependent on packing density.

The laboratory data was also employed to postulate a robust predictive framework for evaluating the overtopping discharge from vertical seawall with additional retrofitting structures. Four empirical-based predictive relations (Eq. 17 - 20) are proposed as a function of geometrical shape, structural configuration and incident wave hydrodynamics, for the retrofitting prototypes tested within this study. Performance of the proposed formulae are evaluated with use of statistical measures. The statistical indexes and comparison of predictive formulae to measured data (Fig.21) confirmed that predictive relations proposed in this study can evaluate the mean overtopping discharge from a vertical seawall with retrofitting robustly with use of appropriate reduction factor based on geometrical shape of the retrofitting structures.

Acknowledgements

This study was funded by the Royal Academy of Engineering – Leverhulme Trust fellowship scheme (LTSRF1516\12\92). Financial support from China Scholarship Council and Sultan Haji Hassanal Bolkiah Foundation has helped this study.

References

Abolfathi, S., Dong, S., Borzooei, S., Yeganeh-Bakhtiari, A., Pearson, J., 2018. Application of Smoothed Particle Hydrodynamics in Evaluating the Performance of Coastal Retrofits Structures. In: Proceedings.of Coastal Engineering doi: https://doi.org/10.9753/icce.v36.papers.109

Abolfathi, S., Pearson, J., 2017. Application of Smoothed Particle Hydrodynamics (SPH) in Nearshore Mixing: A Comparison to Laboratory Data. In: Proceedings.of Coastal Engineering doi: https://doi.org/10.9753/icce.v35.currents.16

Abolfathi, S., Yeganeh-Bakhtiary, A., Hamze-Ziabari, S.M., Borzooei, S., 2016. Wave runup prediction using M5′ model tree algorithm. Ocean Engineering, Volume 112, p. 76-81. https://doi.org/10.1016/j.oceaneng.2015.12.016.

Allsop, N. W. H, 1995. Overtopping performance of vertical and composite breakwaters, seawalls and low reflection alternatives. Paper to Final MAST-MCS Project Workshop, Alderney, UK. University of Hannover.

Allsop, N. W. H., Bruce, T., Pearson, J., Alderson, J., Pullen, T., 2003. Violent wave overtopping at the coast, when are we safe. In:Proceedings of the Conference on Coastal Management. pp. 54-69.

Allsop, N. W. H., Bruce, T., Pearson, J., Besley, P., 2005. Wave overtopping at vertical and steep seawalls. In:Proceedings of the Institution of Civil Engineers-Maritime Engineering. Thomas Telford Ltd, pp. 103-114.

Augustin, L. N., Irish, J. L., Lynett, P. J. C. E., 2009. Laboratory and numerical studies of wave damping by emergent and near-emergent wetland vegetation. Coastal Engineering, 56, 332-340.

Besley, P., Stewart, T., Allsop, N., 1998. Overtopping of vertical structures: new prediction methods to account for shallow water conditions. In: Proceedings of Coastlines, Structures and Breakwaters, London, UK,pp. 46-57.

Bruce, T., Pearson, J., Allsop, W., 2001. Violent overtopping of seawalls-extended prediction methods. Breakwaters, coastal structures and coastlines: In: Proceedings of the international conference organized by the Institution of Civil Engineers and held in London, UK on 26-28 September 2001. Thomas Telford Publishing, pp. 245-255.

Bryant, D. B., Anderson Bryant, M., Sharp, J. A., Bell, G. L., Moore, C., 2019. The response of vegetated dunes to wave attack. Coastal Engineering, 152, 103506.

Chini, N., Stansby, P., Leake, J., Wolf, J., Roberts-Jones, J., Lowe, J., 2010. The impact of sea level rise and climate change on inshore wave climate: A case study for East Anglia (UK). Coastal Engineering, 57**,** 973-984.

Church, J. A., Clark, P. U., Cazenave, A., Gregory, J. M., Jevrejeva, S., Levermann, A., Merrifield, M. A., Milne, G. A., Nerem, R. S., Nunn, P. D., Payne, A. J., Pfeffer, W. T., Stammer, D., Unnikrishnan, A. S., 2013. Sea Level Change. In: Stocker, T. F., Qin, D., Plattner, G.-K., Tignor, M., Allen, S. K., Boschung, J., Nauels, A., Xia, Y., Bex, V. & Midgley, P. M. (eds.) Climate Change 2013: The Physical Science Basis. Contribution of Working Group I to the Fifth Assessment Report of the Intergovernmental Panel on Climate Change. Cambridge, United Kingdom and New York, NY, USA: Cambridge University Press.

Dong, S., Salauddin, M., Abolfathi, S., Tan, Z, H., Pearson, J. M., 2018. The Influence of Geometrical Shape Changes on Wave Overtopping: a Laboratory and SPH Numerical Study. Coasts, Marine Structures and Breakwaters 2017**,** pp. 1217-1226. https://doi.org/10.1680/cmsb.63174.1217

EurOtop 2018. Manual on wave overtopping of sea defences and related structures. An overtopping manual largely based on European research, but for worldwide application. Van der Meer, J.W., Allsop, N.W.H., Bruce, T., De Rouck, J., Kortenhaus, A., Pullen, T., Schüttrumpf, H., Troch, P., Zanuttigh, B. (Available to download from www.overtopping-manual.com).

Feagin, R. A., Furman, M., Salgado, K., Martinez, M. L., Innocenti, R. A., Eubanks, K., Figlus, J., Huff, T. P., Sigren, J., Silva, R. 2019. The role of beach and sand dune vegetation in mediating wave run up erosion. Estuarine, Coastal and Shelf Science, 219, 97-106.

Fitri, A., Hashim, R., Abolfathi, S., Nizam Abd Maulud, K., 2019. Dynamics of sediment transport and erosion-deposition patterns in the locality of a detached low-crested breakwater on a cohesive coast.Water, 11 (8). 1721. doi:10.3390/w11081721

Forbes, K., Broadhead, J., 2007. The role of coastal forests in the mitigation of tsunami impacts, Bangkok, Food and Agriculture Organization of the United Nations.

Formentin, S. M., Zanuttigh, B., 2019a. A Genetic Programming based formula for wave overtopping by crown walls and bullnoses. Coastal Engineering, 152**,** 103529.

Formentin, S. M., Zanuttigh, B., 2019b. Semi-automatic detection of the overtopping waves and reconstruction of the overtopping flow characteristics at coastal structures. Coastal Engineering, 152**,** 103533.

Franco, L., De Gerloni, M., Van der Meer, J., 1995. Wave overtopping on vertical and composite breakwaters. Coastal Engineering 1994.

Goda, Y., 2000. Random Seas and Design of Maritime Structures, World Scientific.

Hall, J., Thacker, S., Ives, M., Cao, Y., Chaudry, M., Blainey, S., Oughton, E., 2017. Strategic analysis of the future of national infrastructure. In: Proceedings of the Institution of Civil Engineers. Thomas Telford 1-9.

Hughes, S. A., Thornton, C. I., Van der Meer, J. W., Scholl, B. N., 2012. Improvements in describing wave overtopping processes. In: Proceedings of Coastal Engineering, 35.

IPCC, 2014. Climate Change 2014: Synthesis Report. Contribution of Working Groups I, II and III to the Fifth Assessment Report of the Intergovernmental Panel on Climate Change, Geneva, Switzerland.

IPCC, 2018. Global Warming of 1.5° C: An IPCC Special Report on the Impacts of Global Warming of 1.5° C Above Pre-industrial Levels and Related Global Greenhouse Gas Emission Pathways, in the Context of Strengthening the Global Response to the Threat of Climate Change, Sustainable Development, and Efforts to Eradicate Poverty, Intergovernmental Panel on Climate Change.

Johnson, H. K. 2006. Wave modelling in the vicinity of submerged breakwaters. Coastal engineering, 53(1), 39-48.

Kisacik D, Troch P, and Van Bogaert P., (2012). Experimental study of violent wave impact on a vertical structure with an overhanging horizontal cantilever slab. Ocean Engineering, 49, 1-15.

Kobayashi, N., Gralher, C., Do, K., 2013. Effects of woody plants on dune erosion and overwash. Journal of Waterway, Port, Coastal, and Ocean Engineering, 139, 466-472.

Kortenhaus, A., Haupt, R., Oumeraci, H., 2002. Design aspects of vertical walls with steep foreland slopes. Breakwaters, Coastal Structures and Coastlines: Proceedings of the International Conference Organized by the Institution of Civil Engineering,, UK. Thomas Telford.

Kortenhaus, A., Pearson, J., Bruce, T., Allsop, N., Van der Meer, J., 2003. Influence of parapets and recurves on wave overtopping and wave loading of complex vertical walls. Coastal Structures, pp. 369-381.

Longuet-Higgins, M. S. J. J., 1952. On the statisticaldistribution of the height of sea waves. Journal of Marine Research, 11, 245-266.

Luhar, M., Infantes, E., Nepf, H., 2017. Seagrass blade motion under waves and its impact on wave decay. Journal of Geophysical Research: Oceans, 122**,** 3736-3752.

MacArthur, M., Naylor, L. A., Hansom, J. D., Burrows, M. T., Loke, L. H., Boyd, I., 2019. Maximising the ecological value of hard coastal structures using textured formliners. Ecological Engineering: X, 1**,** 100002.

Mansard, E. P. & Funke, E. 1980. The measurement of incident and reflected spectra using a least squares method. *Coastal Engineering 1980.*

Martinelli, L., Ruol, P., Volpato, M., Favaretto, C., Castellino, M., De Girolamo, P., Franco, L., Romano, A., Sammarco, P., 2018. Experimental investigation on non-breaking wave forces and overtopping at the recurved parapets of vertical breakwaters. Coastal Engineering, 141**,** 52-67.

Maza Fernandez, M. E., Adler, K., Ramos, D., Garcia, A. M., Nepf, H., 2017. Velocity and drag evolution from the leading edge of a model mangrove forest. Journal of Geophysical Research: Oceans, 122, 9144-9159.

Molines, J., Bayon, A., Gómez-Martín, M. E., Medina, J. R., 2019a. Influence of Parapets on Wave Overtopping on Mound Breakwaters with Crown Walls. Sustainability, 11**,** 7109.

Molines, J., Herrera, M. P., Gómez-Martín, M. E., Medina, J. R., 2019b. Distribution of individual wave overtopping volumes on mound breakwaters. *Coastal Engineering*, 149, 15-27.

Oumeraci, H., Klammer, P., and Partenscky, H.W., (1993). Classification of breaking wave loads on vertical structures. Journal of Waterway, Port, Coastal and Ocean Engineering 119 (4), 381–397.

Pearson, J., Bruce, T., Allsop, W. ,Gironella, X., 2002. Violent wave overtopping–measurements at large and small scale. Coastal Engineering 2002: Solving Coastal Conundrums. Cardiff, UK: World Scientific.

Pearson, J., Bruce, T., Allsop, W., Kortenhaus, A., Van der Meer, J. W., 2004. Effectiveness of recurve walls in reducing wave overtopping on seawalls and breakwaters. Coastal Engineering, 4**,** 4404-4416.

Ravindar, R., Sriram, V. , Schimmels S., Stagonas, D. (2019) Characterization of breaking wave impact on vertical wall with recurve, ISH Journal of Hydraulic Engineering, 25:2, 153-161.

Salauddin, M. Pearson, J. M., 2019. Wave overtopping and toe scouring at a plain vertical seawall with shingle foreshore: A physical model study. Ocean Engineering, 171**,** 286-299.

Salauddin, M., Pearson, J.M., 2020. Laboratory investigation of overtopping at a sloping structure with permeable shingle foreshore. *Ocean Engineering*, 197**,** 106866.

Salauddin, M., O'Sullivan, J., Abolfathi, S., Pearson, J. M., 2020. Extreme wave overtopping at ecologically modified sea defences. 22nd *EGU General Assembly*, 6162**,** doi.org/10.5194/egusphere-egu2020-6162

Tanaka, N., Sasaki, Y., Mowjood, M., Jinadasa, K., Homchuen, S., 2007. Coastal vegetation structures and their functions in tsunami protection: experience of the recent Indian Ocean tsunami. J Landscape Ecological Engineering, 3, 33-45.

Tusinski, A., Verhagen, H. J., 2014. The use of mangroves in coastal protection. Coastal Engineering Proceedings, 1**,** 45.

US Army Corps of Engineers 2008. Coastal Engineering Manual Part VI Chapter 5.

Van der Meer, J. W., Bruce, T., 2013. New physical insights and design formulas on wave overtopping at sloping and vertical structures. Journal of Waterway, Port, Coastal, and Ocean Engineering, 140**,** 04014025.

Van Doorslaer, K., De Rouck, J., 2011. Reduction on wave overtopping on a smooth dike by means of a parapet. Coastal Engineering Proceedings, 1**,** 6.

Van Doorslaer, K., De Rouck, J., Audenaert, S., Duquet, V., 2015. Crest modifications to reduce wave overtopping of non-breaking waves over a smooth dike slope. Coastal Engineering, 101**,** 69-88.

Van Doorslaer, K., De Rouck, J., Van der Meer, J.W., 2016. The reduction of wave overtopping by means of a storm wall. 35th International Conference on Coastal Engineering, 17-20 November 2016 Antalya, Turkey.

Victor, L., Van der Meer, J.W., Troch, P., 2012. Probability distribution of individual wave overtopping volumes for smooth impermeable steep slopes with low crest freeboards. Coastal Engineering, 64**,** 87-101.

Vuik, V., Jonkman, S. N., Borsje, B. W., Suzuki, T. 2016. Nature-based flood protection: the efficiency of vegetated foreshores for reducing wave loads on coastal dikes. Coastal engineering, 116**,** 42-56.

Yeganeh-Bakhtiary, A., Houshangi, H., Abolfathi, S., 2020. Lagrangian two-phase flow modeling of scour in front of vertical breakwater. Coastal Engineering Journal. doi:10.1080/21664250.2020.1747140

Yeganeh-Bakhtiary, A., Houshangi, H., Hajivalie, F., Abolfathi, S., 2017. A numerical study on hydrodynamics of standing waves in front of caisson breakwaters with WCSPH model. Coastal Engineering Journal, 59**,** 1750005-1. DOI: 10.1142/S057856341750005X

Xu, J., Liu, S., Li, J. et al., 2020. Experimental study of wave propagation characteristics on a simplified coral reef. Journal of Hydrodynamics 32, 385–397. https://doi.org/10.1007/s42241-019-0069-2

Yao, Y., Huang, Z., Monismith, S. G., & Lo, E. Y., 2013. Characteristics of monochromatic waves breaking over fringing reefs. Journal of Coastal Research, 29(1), 94-104.

Zanuttigh, B., Van der Meer, J., Bruce, T., Hughes, S. J. P. I., 2013. Coasts, Marine Structures 2013. Statistical characterisation of extreme overtopping wave volumes. In: Proceedings of ICE, Coasts, Marine Structures Breakwaters Conference.

Notation

a, b = coefficients or exponents in formulae [-]

B_r = overhang length of recurve wall [m]

c = shape factor in the Weibull distribution [-]

g = acceleration due to gravity (= 9,81) [m/s²]

Γ =gamma function, [=1/Exp(GAMMALN(1+1/b))]

H_{m0} = estimate of significant wave height from spectral analysis = $4\sqrt{m_0}$ [m]

H_s = significant wave height defined as highest one third of wave heights, $H_s = H_{1/3}$ [m]

$H_{1/3}$ = average of highest third of wave heights [m]

h_s = water depth at (in front of) toe of structure [m]

h_*= discriminator between non - impulsive and impulsive wave overtopping, $h_* = \frac{h}{H_{m0}} \frac{h}{L_{m-1,0}}$ [-]

h_r= height of recurve wall [m]

k_{23}= minimum *k*-factor of recurve wall, which is set to 0.20 [-]

$L_{m-1,0}$ = deep water wave length based on $T_{m-1,0}$. $L_{m-1,0}=gT^2_{m-1,0}/2\pi$ [m]

L_0 = deep water wave length based on Tm. $L_0 = gT^2/2\pi$

N_{ow} = number of overtopping waves [-]

N_w = number of incident waves [-]

P_c = distance from bottom of recurve to still water level (SWL) [m]

P_{ov}= Proportion of overtopping waves. Calculated with N_{ow}/N_w

q = mean overtopping discharge per meter structure width [m^3/m/s]

R_c = crest freeboard of structure [m]

$s_{m-1,0}$= wave steepness with $L_{m-1,0}$, based on $T_{m-1,0}$. $s_{m-1,0}=H_{m0}/L_{m-1,0} = 2\pi H_{m0}/(gT_{m-1,0}{}^2)$ [-]

T_m = average wave period from time - domain analysis [s]

$T_{m-1,0}$ = spectral period defined by m - $1/m_0$ [s]

V_{max}= maximum individual overtopping discharge per structure width [m^3/m]

List of Tables

Table 1. Nominal wave conditions used for the physical tests (1:50 scale)

Vertical seawall condition						
Water depth (m)	0.07	0.1	0.13	0.07	0.1	0.25
Relative freeboard	0.75 - 2.5			2.8 - 3.9		
Input wave period (s)	1.21-1.65			1.16-1.65		
Significant wave height (m)	0.075 - 0.140			0.047 - 0.078		

Table 2. RMSE values of regression equations fitted based on tested retrofitting structures.

	RMSE		
	Rc/Hm0<1.35	Rc/Hm0>1.35	All tested conditions
Reef Breakwater	0.239	0.580	0.527
Diffraction Pillars	0.205	0.186	0.190
Recurve Wall	0.488	0.504	0.500
Vegetation	0.234	0.252	0.248

List of Figures

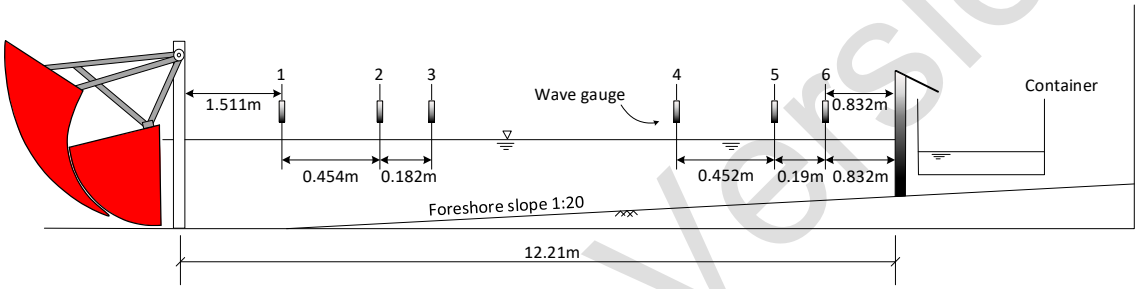

Figure 1. Schematic of experimental setup for the vertical wall (base case)

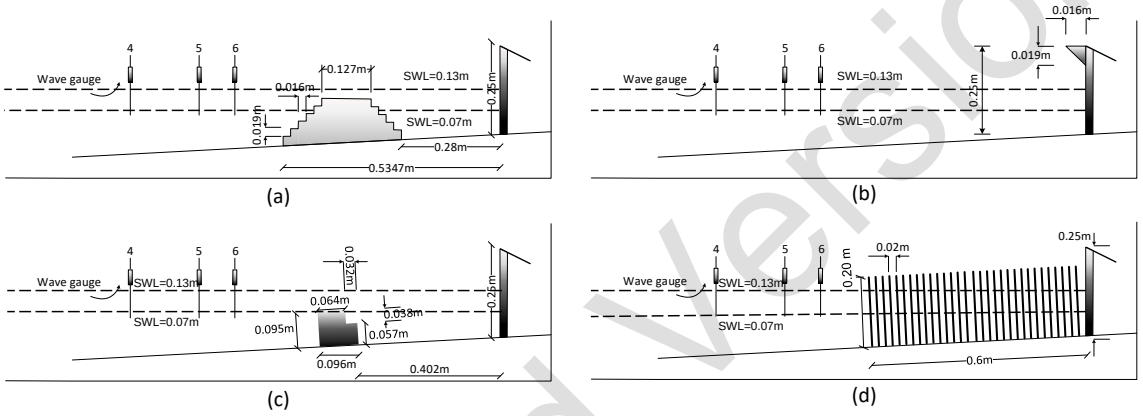

Figure 2. Experimental setup for retrofit solutions, (a) Cross-section of the reef breakwater (b) Cross-section of the recurve wall (c) Cross-section of the diffraction pillars [0.095m width, 0.07m between per pillar] (d) Cross-section of the vegetation

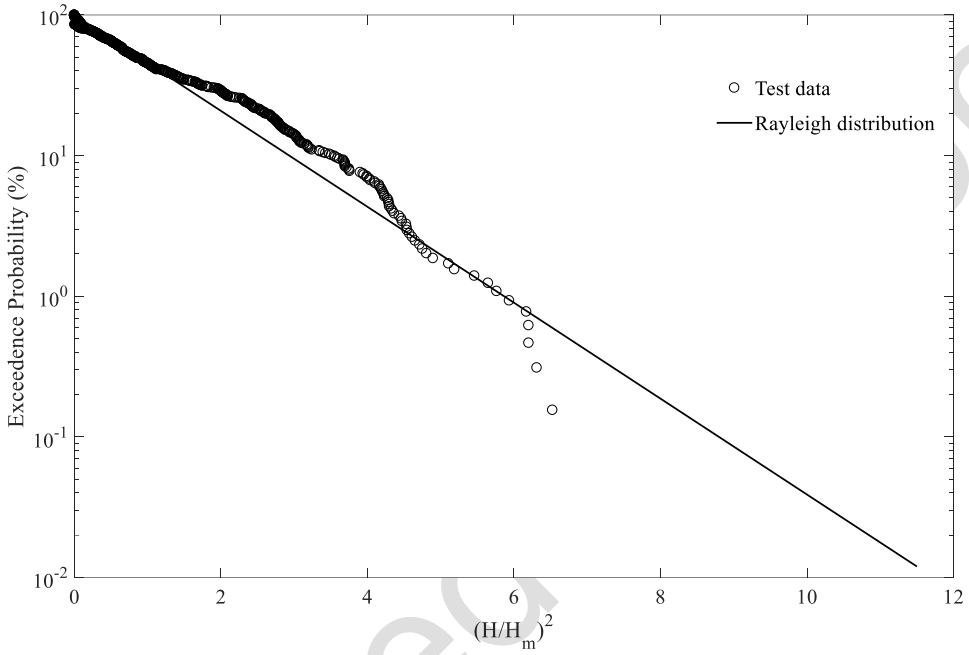

Figure 3.a Validation of individual wave height with Rayleigh distribution, Test condition: h_s=0.07m, T_p=1.50s, relative freeboard=2.37, H_s=0.076m

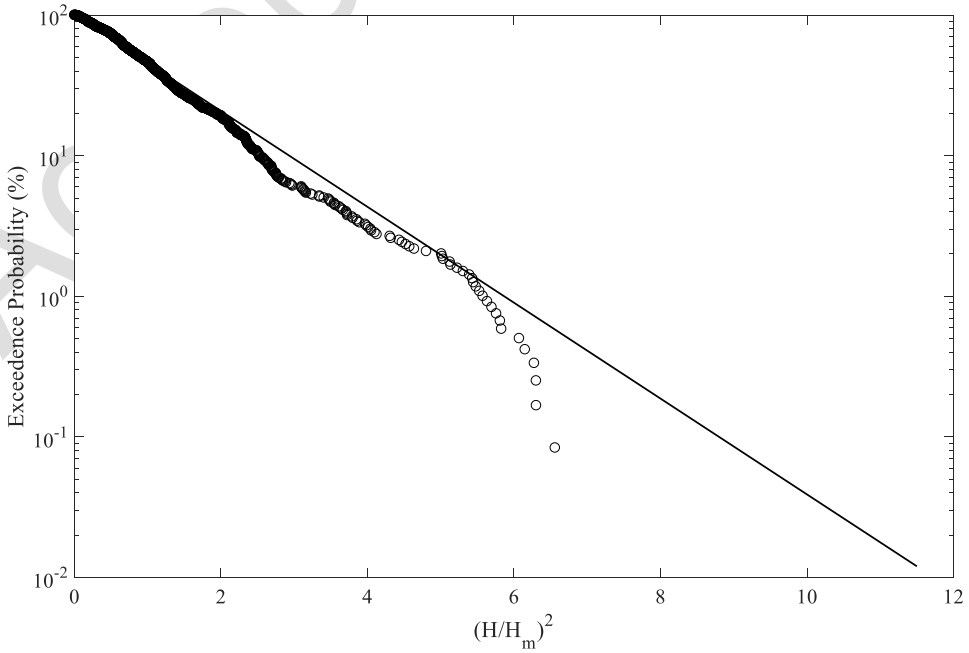

Figure 3.b Validation of individual wave height with Rayleigh distribution, Test condition: h_s=0.10m, T_p=1.25s, relative freeboard=1.69, H_s=0.089m

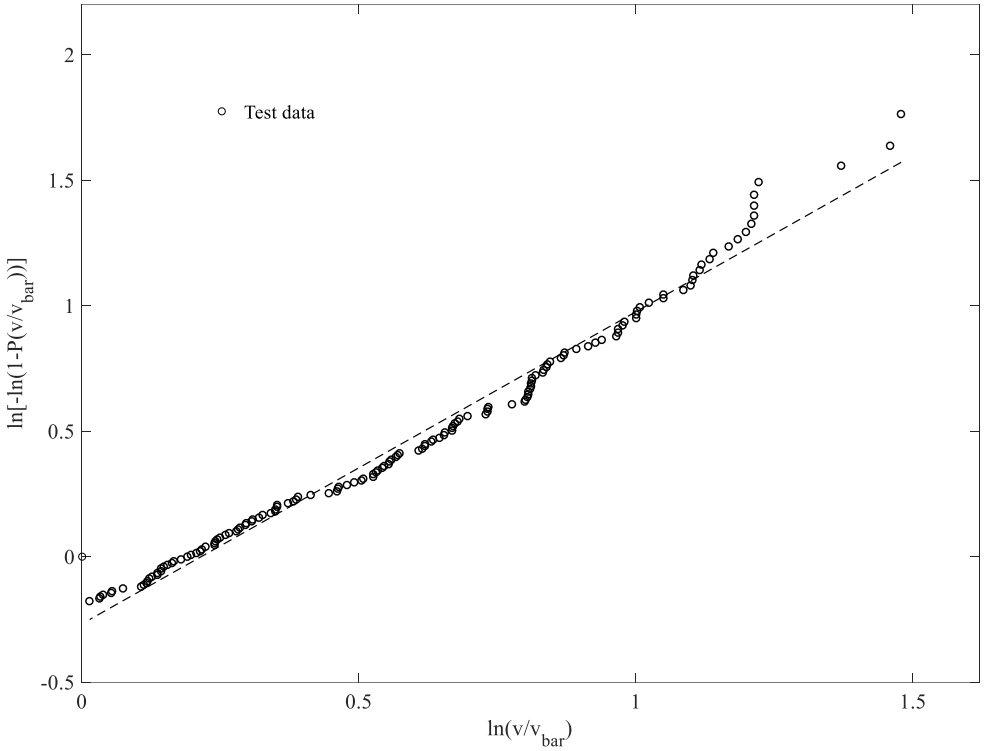

Figure 4.a Comparisons between individual overtopping volume distribution and Weibull distribution, Test with h_s =0.07m, T_p=1.50s

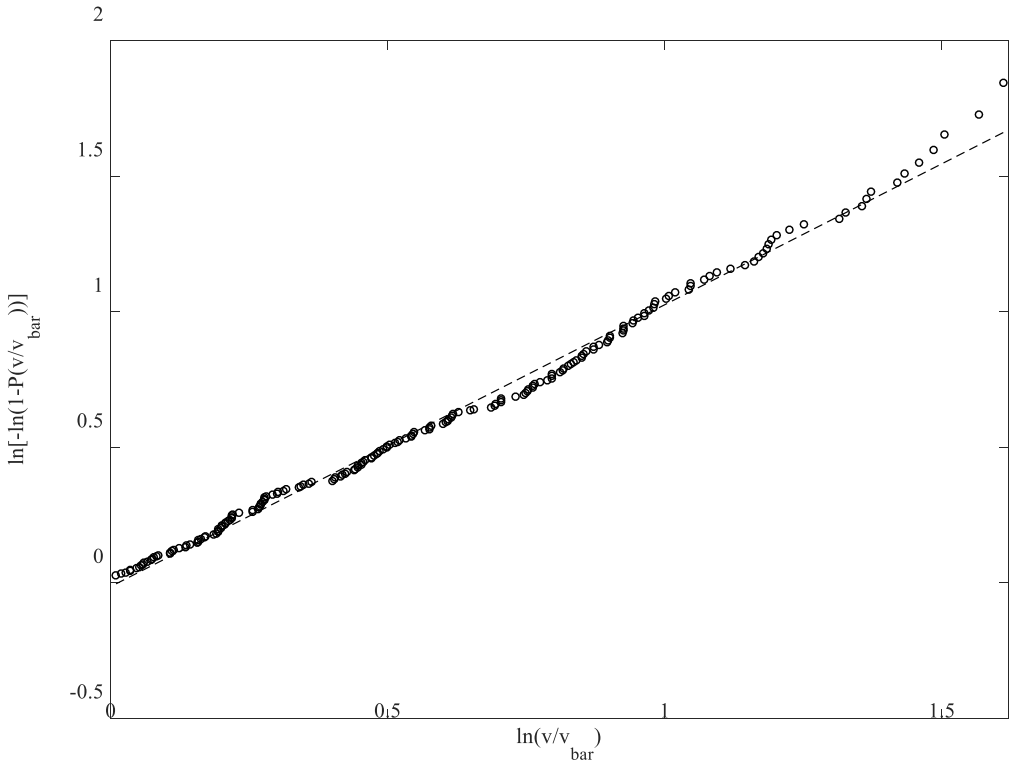

Figure 4.b Comparisons between individual overtopping volume distribution and Weibull distribution, Test with h_s=0.10m, T_p=1.25s

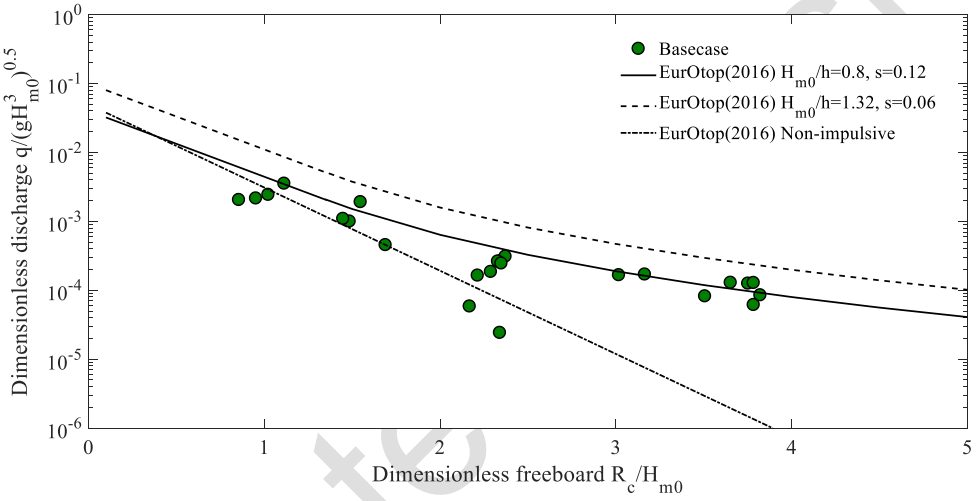

Figure 5. Mean overtopping discharge from the plain vertical wall.

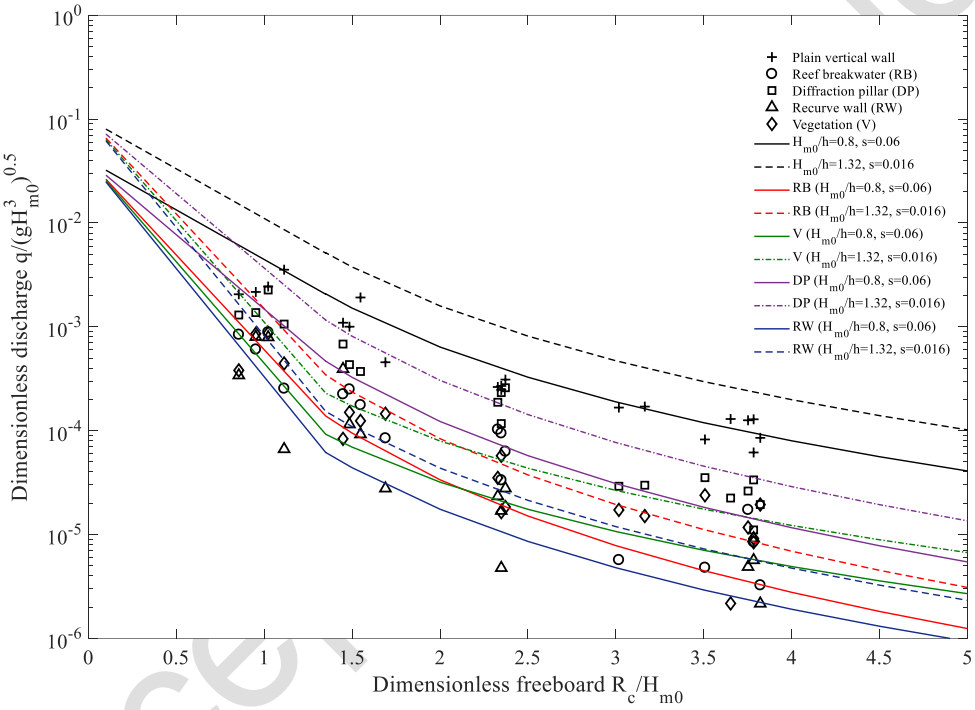

Figure 6. Mean overtopping discharge on vertical wall with retrofit solutions (impulsive conditions)

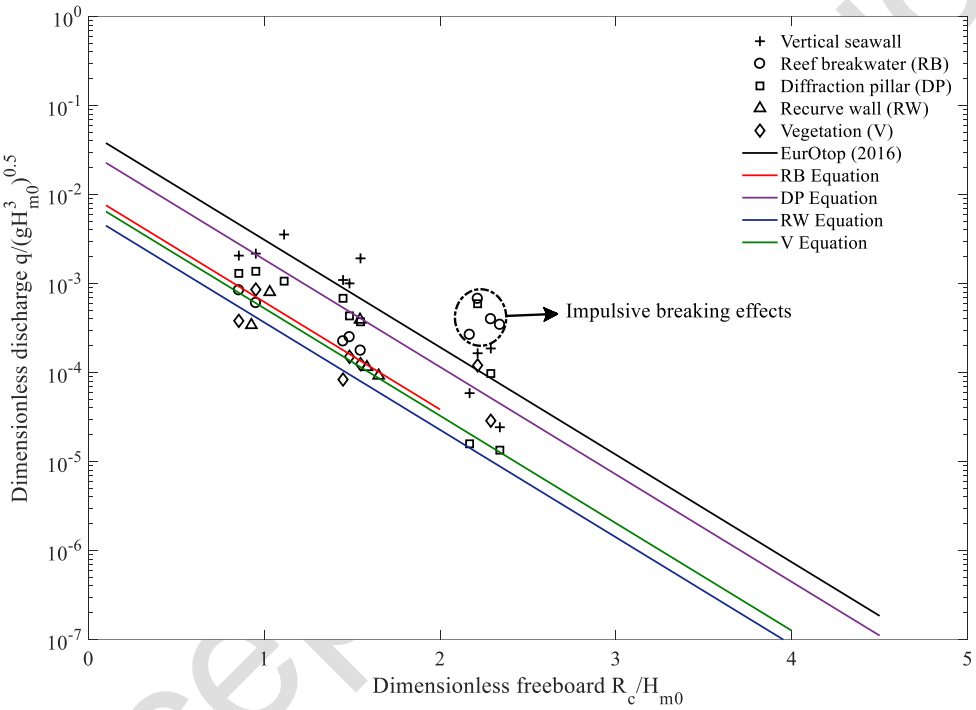

Figure 7. Mean overtopping discharge on vertical wall with retrofit cases and comparison to EurOtop (2018) for non-impulsive conditions

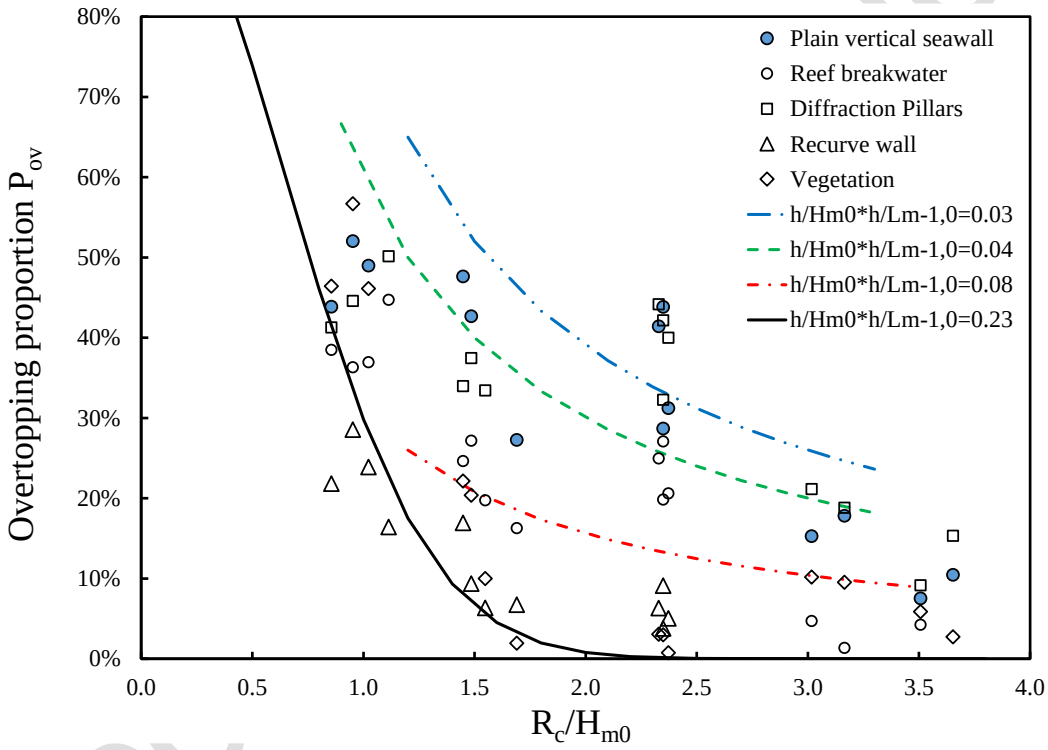

Figure 8. Proportion of overtopping waves from vertical seawalls with retrofit solutions

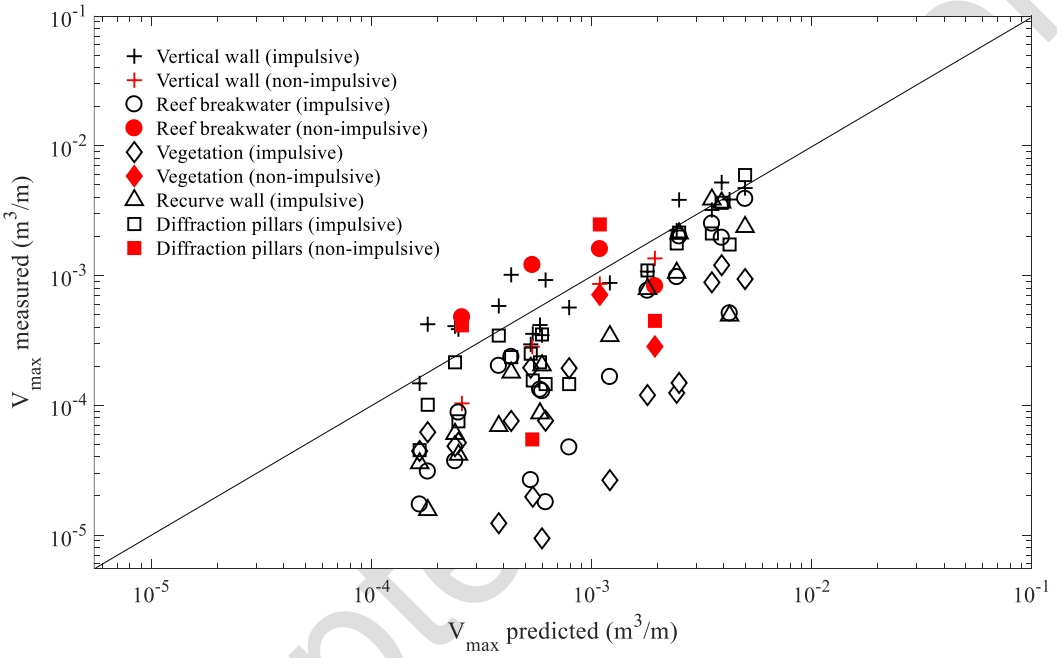

Figure 9. Maximum individual overtopping volumes of retrofit structures compared with existing empirical predictions

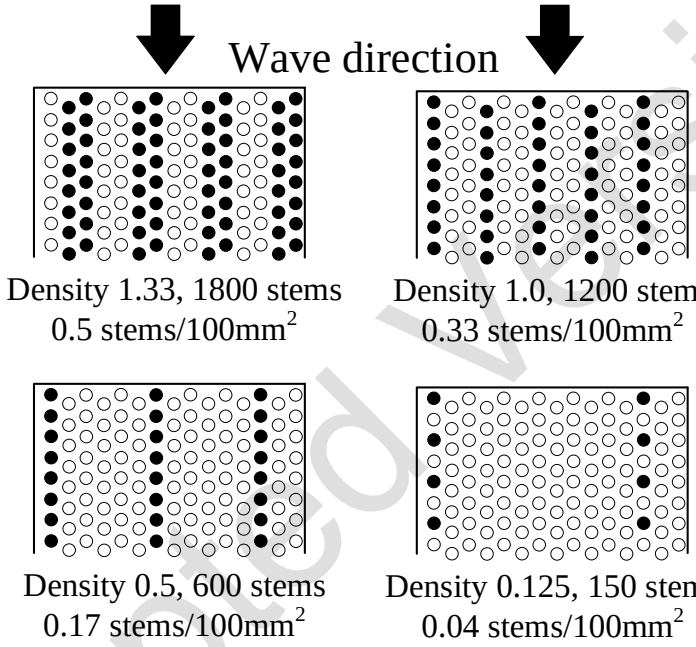

Figure 10. Schematic of four tested packing densities of vegetation (top view)

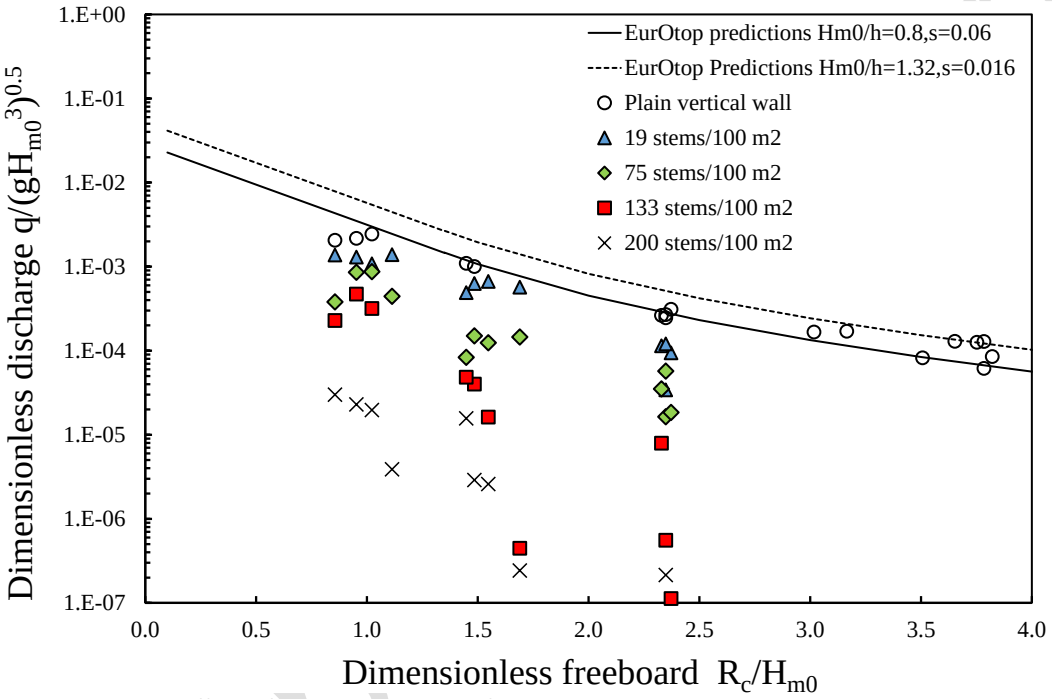

Figure 11. Effects of the packing density of the vegetation on the mean overtopping discharge

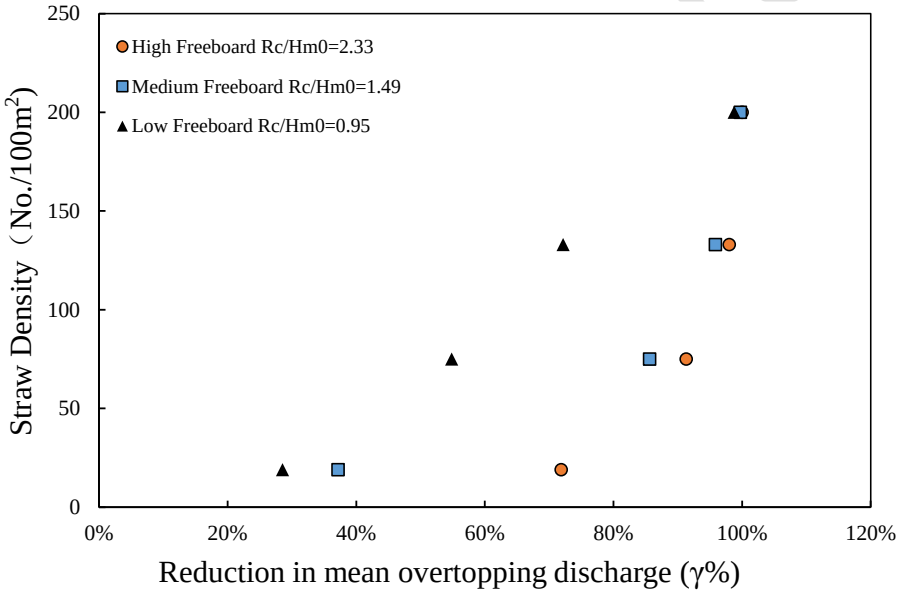

Figure 12. Relationship between reduction γ% in mean overtopping discharge and packing density of vegetation.

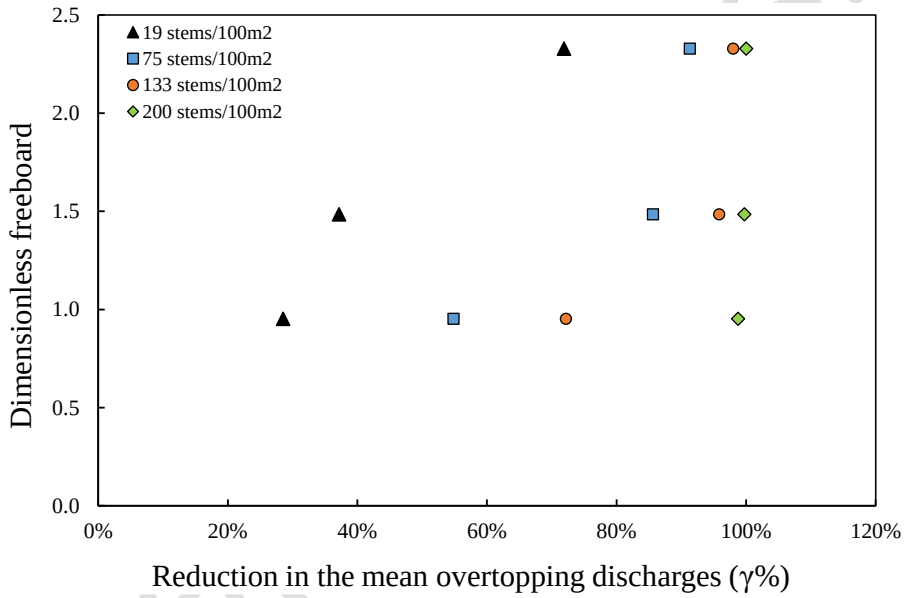

Figure 13. Relationship between reduction γ% in mean overtopping discharge and dimensionless freeboard

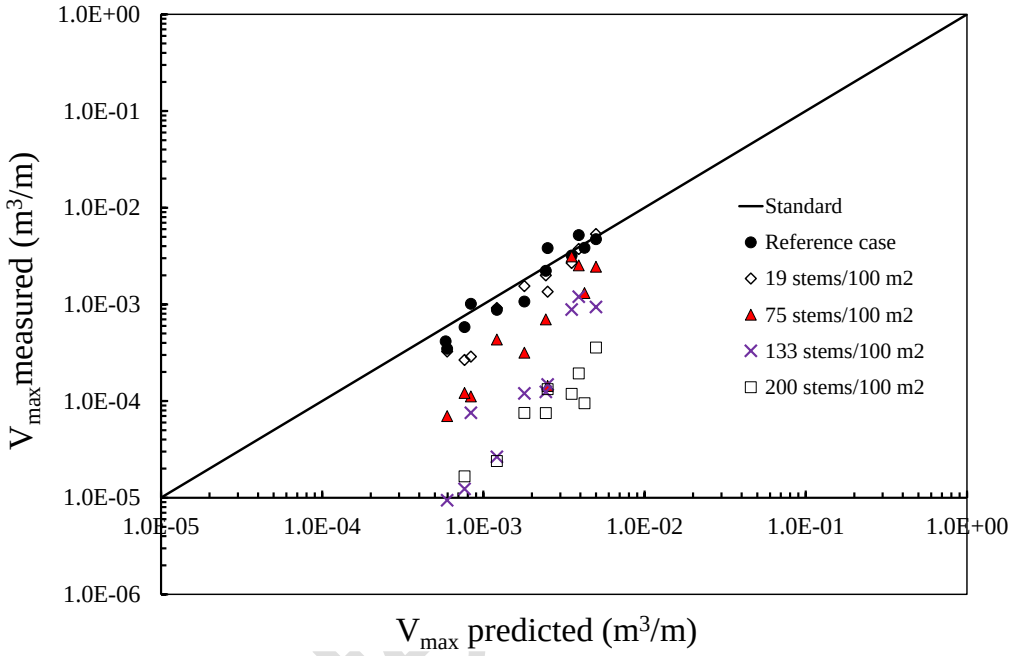

Figure 14. Maximum individual discharge form reference case and four tested vegetation configurations

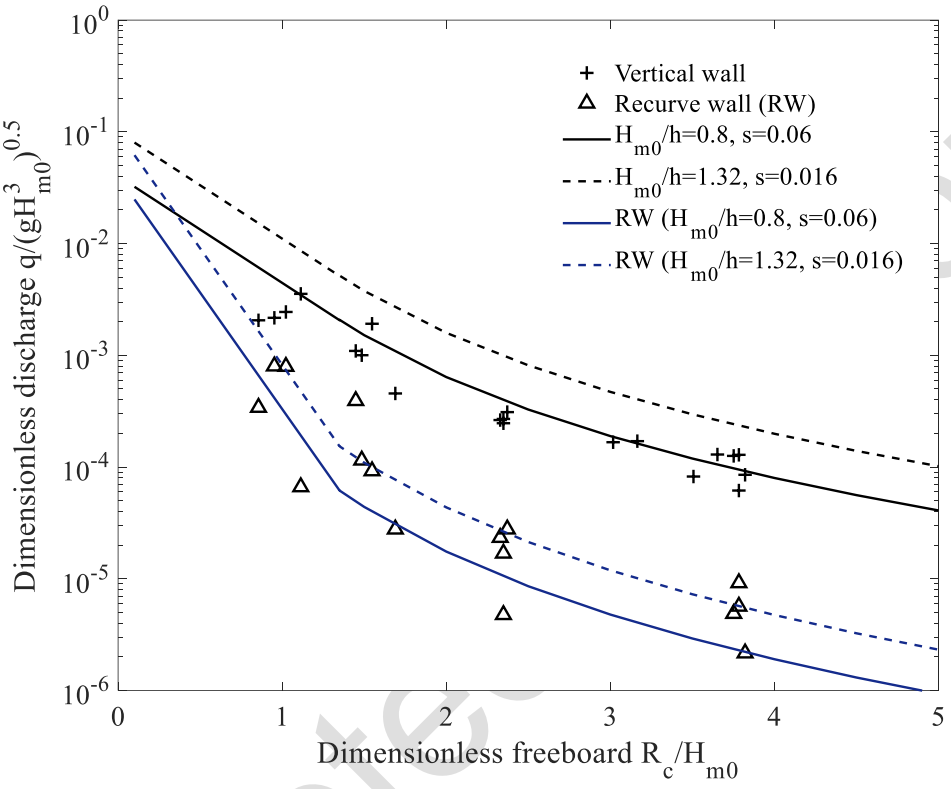

Figure 15. Mean overtopping discharges on plain vertical seawall and the recurve wall (impulsive conditions).

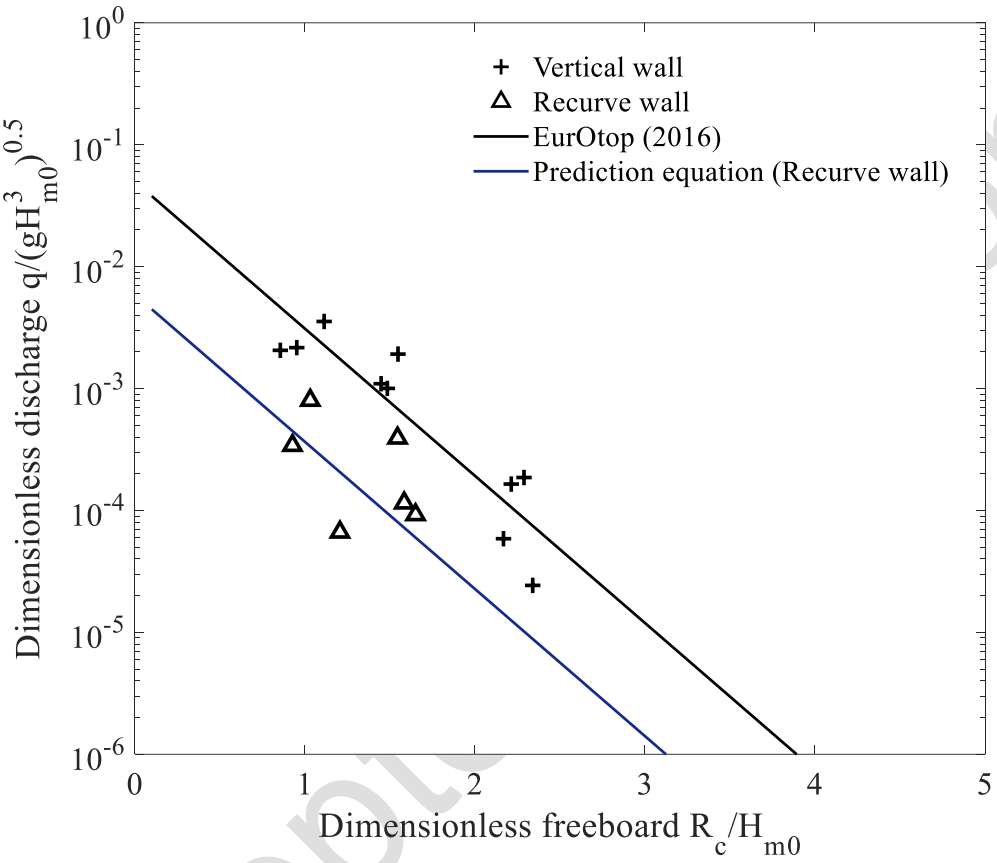

Figure 16. Mean overtopping discharges on plain vertical seawall and the recurve wall for the non-impulsive conditions and comparison with EurOtop (2018)

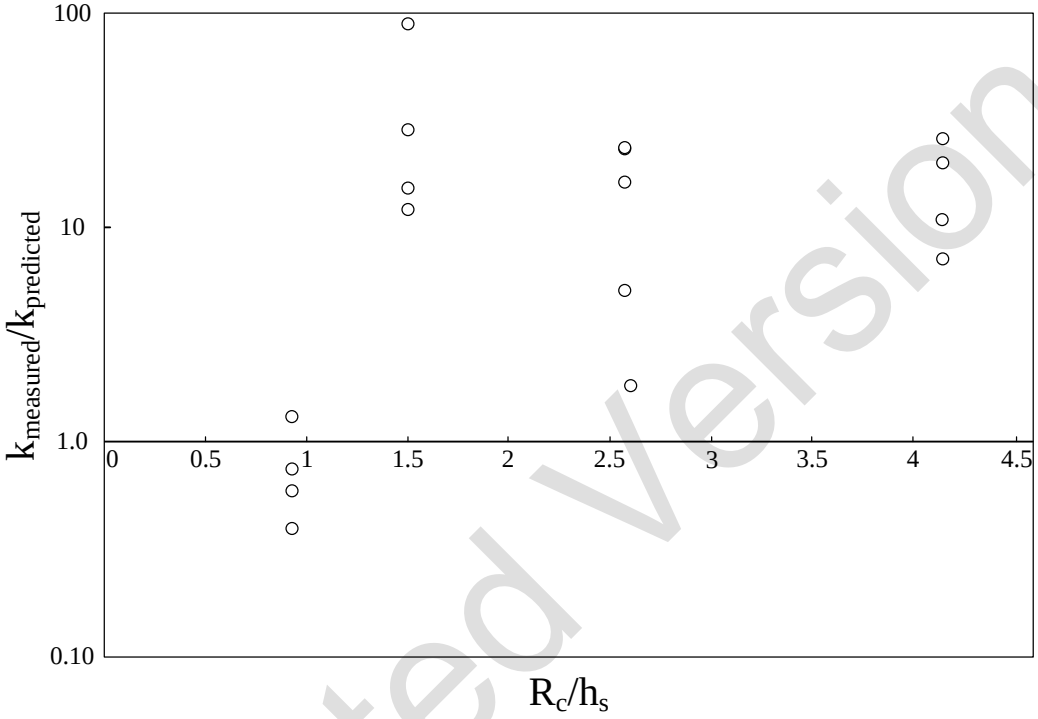

Figure 17. Comparisons between measured and predicted mean overtopping discharges on recurve wall

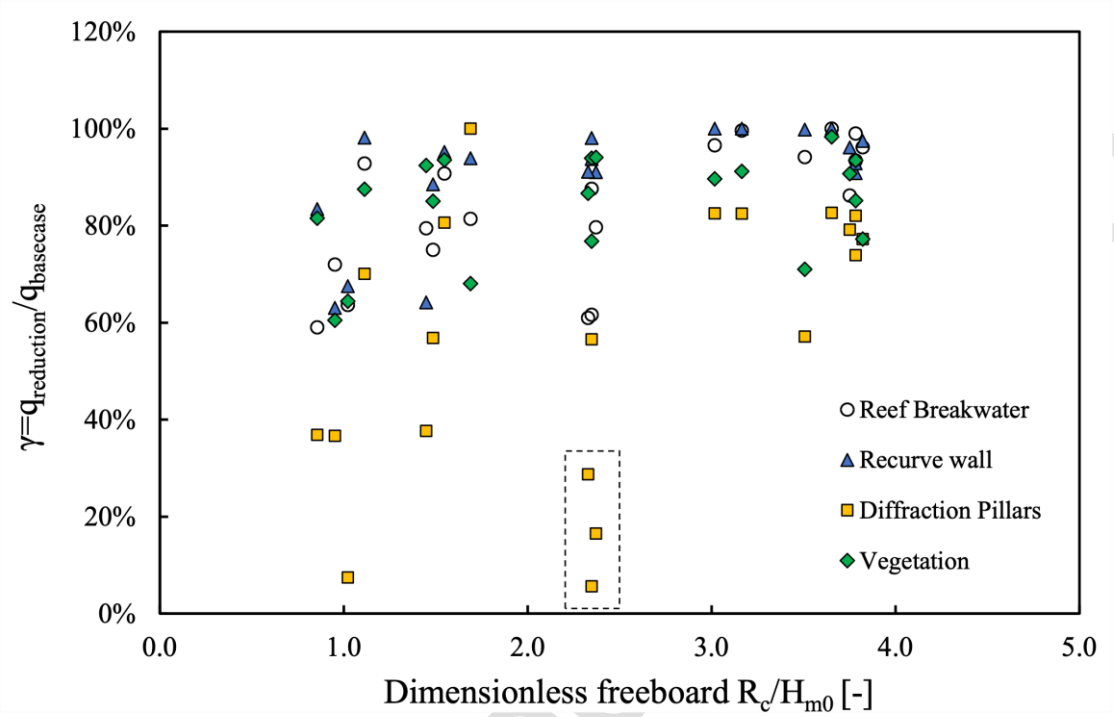

Figure 18. Measured reduction in mean overtopping discharge for all four retrofits

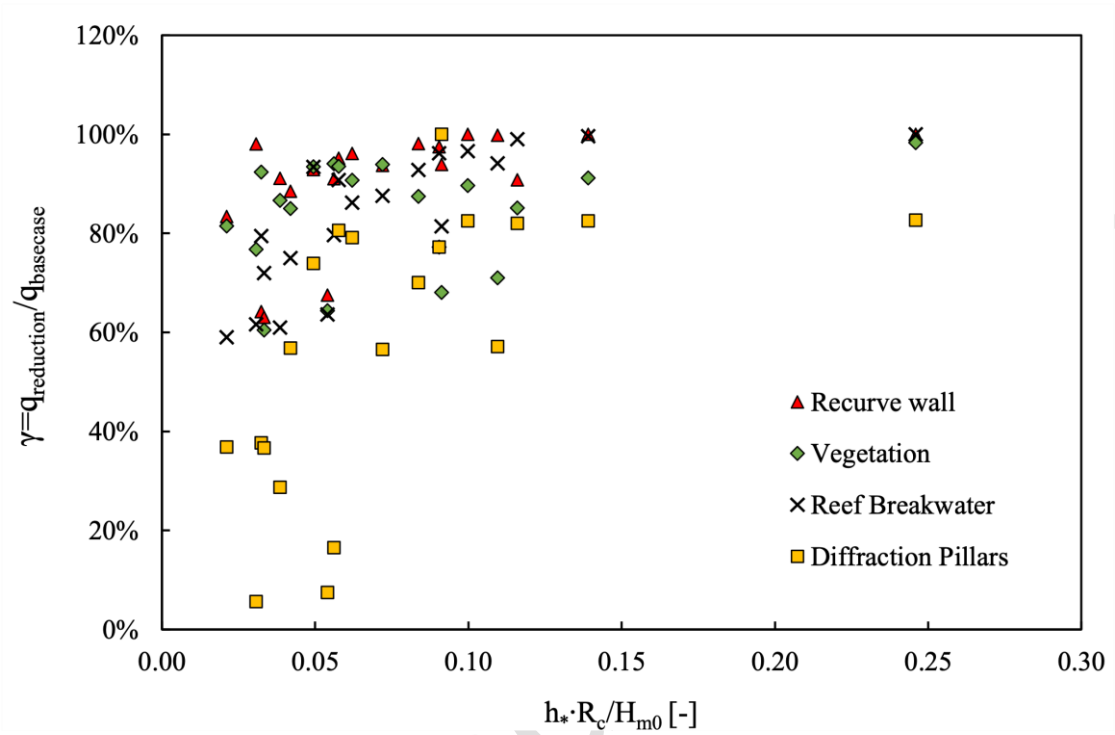

Figure 19. Combined influence of h_* and R_c/H_{m0} to the reduction of mean overtopping discharge

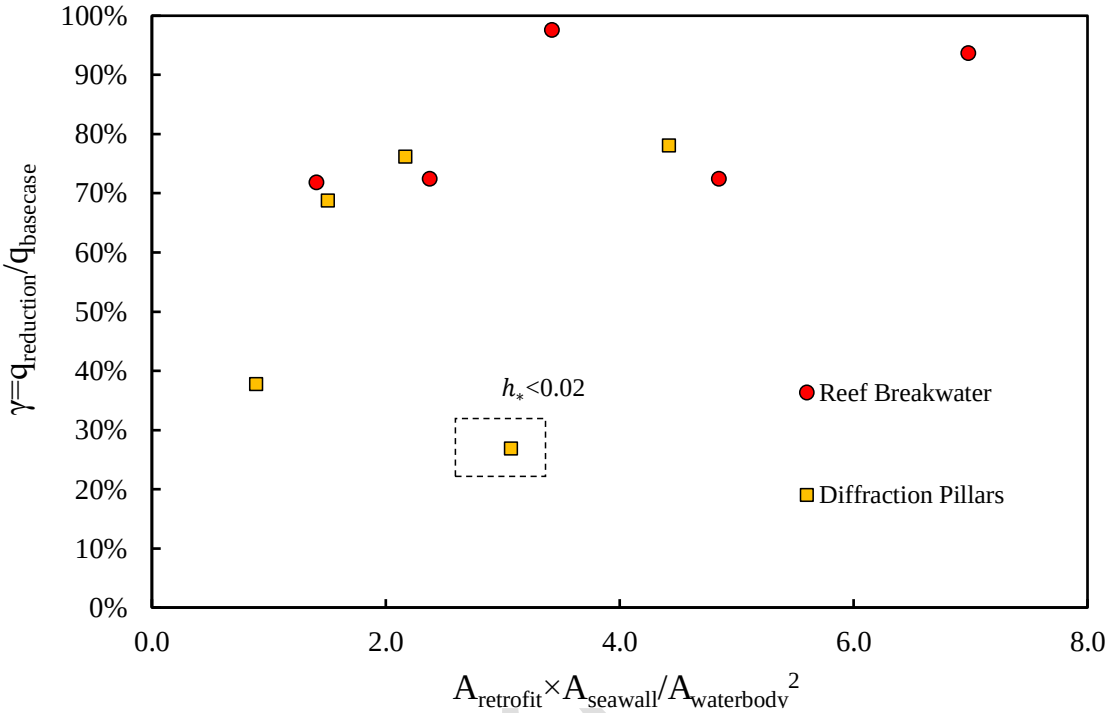

Figure 20. Relationship between reductions in mean overtopping discharge and dimensionless area of retrofits.

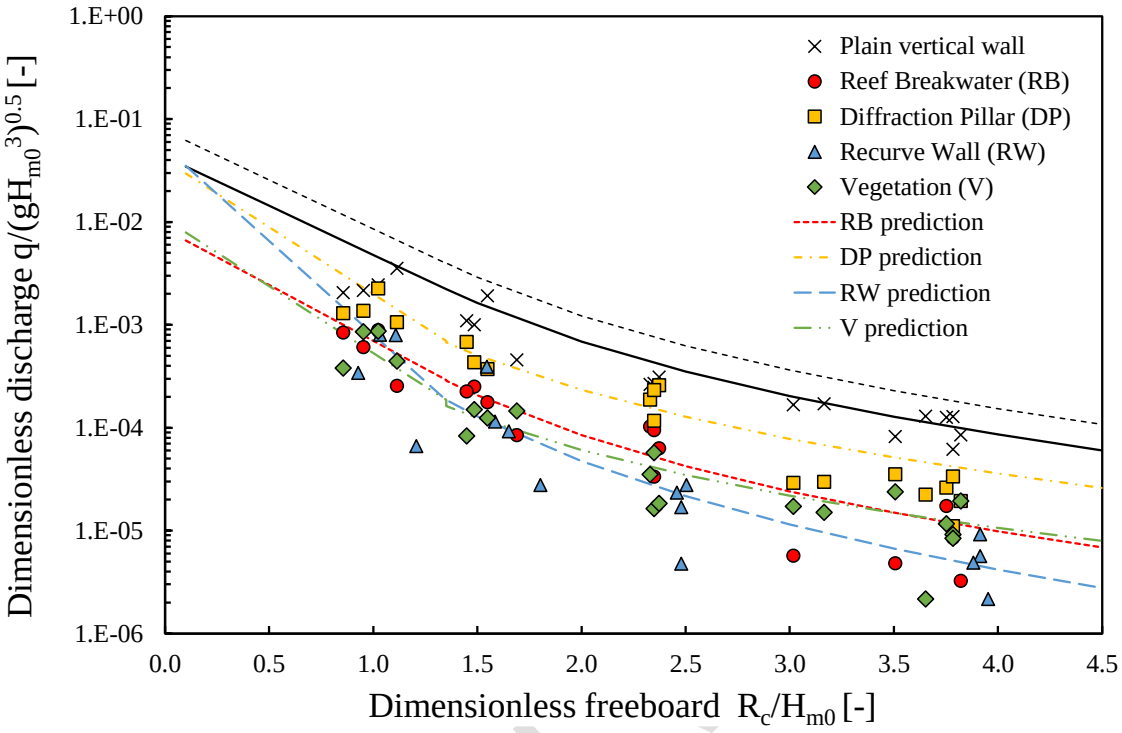

Figure 21. Modified regression equations based on EurOtop (2018) for the impulsive mean overtopping discharges from retrofitting configurations